Nagaoka University of Technology

Doctoral Thesis

Spatial distribution of earthquake-induced landslides in the 2004 Mid-Niigata Prefecture earthquake and identification of shear strength and seismic coefficient by surficial landslides record

Author:
Surangani Bandara

Supervisor:
Professor Satoru Ohtsuka

A thesis submitted in partial fulfillment of the requirements for the degree of Doctor of Engineering

in the

Energy and Environment Science

Examination committee: Prof. Ohtsuka Satoru
Prof. Mitsutaka Sugimoto
Assoc. Prof. Hirofumi Toyota
Assoc. Prof. Yasuyuki Miyaki
Assoc. Prof. Yu Otake

Department of Civil and Environmental Engineering
Nagaoka University of Technology
JAPAN 2017

Declaration

I, Surangani Bandara, declare that this thesis titled "Spatial distribution of earthquake-induced landslides in the 2004 Mid-Niigata Prefecture earthquake and identification of shear strength and seismic coefficient by surficial landslide record" and the work presented in it, are my own. I confirm that:

- This work was done wholly or mainly while in candidature for a research degree at this university
- Where any part of this thesis has previously been submitted for a degree or any other publication, this has been clearly stated
- Where I have consulted the published work of others, this is always clearly attributed
- Where I have quoted from the work of others, the source is always given. With the exception of such quotations, this thesis is entirely my own work
- I have acknowledged all main sources of help

....

Student's signature Date

I certify that I have read this dissertation and that, in my opinion, it is fully adequate in scope and quality as a dissertation for the three year degree of Doctor of Engineering.

....

Supervisor's signature Date

(Prof. Satoru Ohtsuka)

Abstract

The 2004 Mid-Niigata prefecture earthquake with a moment magnitude of 6.8 occurred in the Chuetsu area of Niigata prefecture in Japan. This catastrophic earthquake was followed by severe aftershocks and caused many types of landslides such as surficial slides, shallow slides, and deep slides.This study investigates the correlations between each type of landslide and the bedding plane orientation and dip, and other geomorphologic conditions. The landslide occurrence ratio (LOR) is used as an index to determine the correlation between the earthquake-induced landslides and the slope angle, slope aspect, rock type, bedding plane orientation and dip, and distance from the epicentre fault line.

Even though the bedding planes are a known factor that controls the landslides it is hard to obtain information on bedding attitude for large areas through field surveys because they are time-consuming and resource intensive. Therefore we propose a GIS-based method to estimate geometric alignment between topography and the orientation of geologic bedding planes. Computation of the topographic/bedding-plane alignment requires the derivation of four spatially distributed variables: topographic slope, slope aspect, bedding dip, and bedding dip direction. Slope and slope aspect surfaces are derived from the (10 m) digital elevation model. Inverse distance weighting (IDW) is used to interpolate dip direction and dip angle from point measurements of strike and dip. Using these four variables, slopes are classified into three functional types. The method provides an efficient means of estimating the topography/bedding plane relationship over large areas.

Pseudo-static analysis can identify as one of the approaches used in engineering practice to clarify the seismic response of embankments and slopes. The most important aspect of the Pseudo-static analysis method is to select an appropriate seismic coefficient. In order to investigate this, a parametric study was performed on a surficial slide of varies slope angles and soil properties subjected to strong ground motion during the earthquake. The proposed back analysis procedure was employed by assuming that the soil properties as random variables owing to the uncertainties. In addition to that, the soil properties are assumed as remaining constant over the analysis domain. The variation in seismic response characteristics of the slope is represented by the distance from the epicentre fault line. Since the analysis of 4504 recorded surficial slides clearly shows a unique relationship with slope angle and epicenter fault line, this property enhances calculating the shear strength of the weathered soil covering slopes and the horizontal seismic coefficient through back analysis procedure.

Acknowledgements

First and foremost I would like to express my sincere gratitude to my academic advisor Professor Storu Ohtsuka. It was a great pleasure and my very good fortune to work with him. I am especially grateful to him for bringing me into the world of "Landslides" and his trust in me always, which has helped me to build my confidence. I appreciate his continuous support during my PhD study and research. I admire him not only because of his immense knowledge but also because of his great personality. He is such an open-minded and caring person with seemingly unlimited patience. All I have learned from him is a priceless treasure for the rest of my life.

I am also heartily thankful to Professor Mitsutaka Sugimoto, Associate Professor Hirofumi Toyota, Associate Professor Yasuyuki Miyaki, and Associate Professor Yu Otake (Niigata University) for their suggestions and active discussions as committee members of my doctoral examination.

Furthermore I would also like to thank the members of my laboratory for their support and encouragement at all times. Last but not the least; I would like to thank my family. They were always supporting me and motivating me with their best wishes.

"This dissertation is first dedicated to my brilliant and outrageously loving and supportive husband, Sagara Nirmal Sumathipala, Ph.D. Second, I dedicate this to our exuberant, sweet daughter Akeila Evangeline Sumathipala for the sacrifices she made. Third, I dedicate this to my parents for giving me strength and love. . . . . "

Contents

List of Figures

List of Tables

Abbreviations

LOR	**L**andslide **O**ccurrence **R**atio
JST	**J**apanese **S**tandard **T**ime
JMA	**J**apan **M**eteorological **A**gency
GIS	**G**eographic **I**nformation **S**ystem
SW	**S**outh **W**est
NE	**N**orth **E**ast
NW	**N**orth **W**est
DEM	**D**igital **E**levation **M**odel
IDW	**I**nverse **D**istance **W**eighted
PHA	**P**eak **H**orizontal **A**cceleration
JCOLD	**J**apan **C**ommission **O**n **L**arge **D**ams
PS	**P**seudo-**S**tatic
COV	**C**oefficient **O**f **v**ariation

Chapter 1

Introduction

1.1 Introduction

Japan is a seismically active island nation which is surrounded by mountain ranges running through each of the main islands. Japan has long been at risk of earthquakes and related disasters due to its geological location at the intersection of three tectonic plates: the Pacific Plate, the Philippine Sea Plate, and the Eurasian plate which is located in a volcanic zone on the Pacific Ring of Fire. Earthquake can be identified as the main triggering factor of many types of hazards such as ground shaking, surface faulting, landslides, liquefaction, and tsunamis. Of these, landslides can be distinguished as one of the most destructive geo-hazards. They usually occur suddenly, destroy critical infrastructure and ecological systems, and cause large-scale damage to buildings, as well as cause human casualties and economic losses. For example, large earthquakes have the capability of triggering thousands of landslides which in turn can cause extensive damage and loss of lives (Keefer, 1984) [34].

At the Japanese Standard Time (JST) 17:56 on October 23, 2004 an earthquake with a moment magnitude of 6.8 struck Mid-Niigata prefecture in Japan and caused many landslides and slope failures in the Chuetsu region of Niigata prefecture. The location of the hypocenter was 37°17.4′N, 138°52.2′E, at a depth of 13 km (Japan Meteorological Agency (JMA), 2004) [1]. This catastrophic earthquake caused extensive damage in an epicentral area including Ojiya City, Nagaoka City, and Yamakoshi village. The earthquake claimed more than 60 lives and approximately 103,000 people sought refuge;

16,000 houses were destroyed (Niigata Prefectural Government, 2009) [24]. **Figure 1.1** shows the examples of damage to roads and buildings in Chuetsu region;(a) Buildings and roads damage due to the slope failures in the Yamakoshi village (taken by Ohtsuka S), (b)Tunnel damage due to the open and cracked walls and sediment flowing in Ojiya Kawaguchi Kisawa line (taken by Sanko Consultant Co., Ltd), (c) JR Joetsu line damage due to the collapse of the valley filling embankment (taken by JR East Japan, photographed in Yuzawa direction from Nagaoka direction), and (d) Roads and houses damage in Ojiya City (taken by Taken T). This event provides a unique opportunity to study the earthquake-induced landslides in order to obtain a better understanding of their causal factors and spatial distribution.

The various types of landslides can be differentiated based on types of movement, involved material, mechanism of initiation, or any other principles that have been proposed by many authors. The landslide classification of Varnes (1954, 1978) [66, 67] and Hutchinson (1968, 1988) [29, 30] are employed worldwide. After the 2004 Mid-Niigata prefecture earthquake, many companies, government institutions, and universities conducted investigations in damaged areas. Among them The National Research Institute for Earth Science and Disaster Prevention has classified the earthquake-induced landslides according to the depth of the slip surface, failure type, and materials of the moving body (Inokuchi et al., 2008) [46]. Based on the depth of the slip surface, the following three major landslide types were identified: surficial slide (depth $\leq$1m), shallow slide (depth between 1m and 10m), and deep slide (depth $\geq$10m). These three types of landslides were further classified in detail as rotational and translational in character. Inokuchi et al. (2008) [46] conducted five field surveys of the study area lasting 3 years after the earthquake and studied aerial photographs in detail to clarify the validity of landslide classification. In this study, these three main landslide types were studied to distinguish their spatial distribution by correlating the landslide occurrence ratio (LOR) with the physical parameters that control the seismic stability of slopes.

In addition to examining the spatial distribution of earthquake-induced landslide, it is essential to consider the seismic effects for designing slope stability, retaining walls, bridges, and other engineering structures. It is important to determine the shear strength parameters on a failure surface for stability evaluation and engineering analysis of a landslide, as these parameters are mainly determined by the test, back analysis method and

FIGURE 1.1: Landslide damage on roads and buildings in Chuetsu region

engineering experience analogy method (Sonmez et al., 1998) [63]. Among these methods, the back calculation is a procedure which offers the opportunity to estimate the shear strength properties along the failure surface by the mathematical method. Soil strength calculation by back analysis avoids many of the problems related to laboratory testing and is widely used, especially in association with landslide repair studies (Duncan and Stark, 1992) [20]. This thesis presents the rational procedure to calculate the horizontal seismic coefficient according to the distance from the epicenter fault line and shear strength of the weathered soil. The seismic coefficient is found similar with past research works.

1.2 Research Objectives

The general purposes of the thesis research presented is to: firstly, obtain a more comprehensive understanding of the relation between each landslide types and causative factors; and secondly, calculate shear strength parameters of weathered soil and seismic coefficient. To fulfill these objectives the following sub-objectives are also considered. The study combined different methodologies and approaches of investigating bedding

influence for the occurrence of landslides. It aims to provide a comprehensive methodology to calculate geometric alignment between topography and the orientation of geologic bedding planes for long-term landslide hazard assessment. This research conducted back analysis for different case studies by assuming that the seismic coefficient varies with distance from the epicenter fault line. It aims to calculate seismic coefficient and shear strength of the weathered soil and these back calculated values can be used to analysed the stability of other slopes in the same geological formation.

1.3 Thesis Outline

This thesis consists of seven chapters. **Chapter 1** starts with the introduction and research objectives. **Chapter 2** reviews previous research on landslide distribution related with geologic and geomorphologic parameters. The second part of the chapter briefly describes the earthquake characteristics and finally reviews previous research on slope failures triggered by the Mid-Niigata prefecture earthquake. Detailed description of the study area and data preparation approaches are presented in **Chapter 3**. **Chapter 4** discusses the preliminary statistical analysis of spatial distribution of earthquake-induced landslides. **Chapter 5** begins by introducing a methodology to estimate bedding attitude. In this chapter, three main landslide types were analyzed in detail to characterize their spatial distribution by correlating LOR with geologic and geomorphologic factors. In **Chapter 6**, back analysis is introduced to calculate the shear strength of the weathered soil and seismic coefficient. **Chapter 7** evaluates the overall findings of the research and concludes the findings with recommendations for future work on this topic.

Chapter 2

Literature Review

2.1 Influential Factors on Landslide Distribution

There are many factors that affect slope stability and landslide distribution. Sidle and Ochiai (2006) [62] identified five types of natural factors which influence the landslide, i.e. seismicity; strength, chemistry, and mineralogy of soil; geology; geomorphology; and hydrology. Studying the causative factors for landslides which are triggered by an earthquake is an essential subject for understanding which areas could be more prone to land sliding in a future earthquake. Many researchers analyzed the correlations of landslide occurrence with slope steepness, distance from the earthquake source, and rock types or geology, respectively (e.g. Keefer, 2000; [35] Parise and Jibson, 2000; [48] Khazai and Sitar, 2003; [36] Wang et al., 2007; [68] Sato and Harp, 2009; [56] Qi et al., 2010; [50] Papathanassiou et al., 2013; [47] Basharat et al., 2014; [4] Xu et al., 2014; [73] and Xiaoli et al., 2015 [72]).

Keefer (2000) [35] mapped 1280 landslides that were triggered by the 1989 Loma Prieta earthquake (Mw 6.9). The study shows the landslides induced by an earthquake are possibly correlated with slope steepness, distance from a source, and rock types. Harp and Jibson (1996) [28] identified more than 11000 landslides, which had been triggered by the 1994 Northridge earthquake (Mw 6.7), California. According to their findings, the most common types of the landslide triggered by the earthquake were highly disrupted, shallow falls and slides of rock and debris. Parise and Jibson (2000) [48] have described landslide morphologies by computing simple morphometric parameters (i.e. area, length,

width, aspect ratio, slope angle) and statistically quantified and ranked the susceptibility of each geologic unit to seismically induced landslides. Wang et al. (2002, 2003 a,b) [69–71] and Chigira et al. (2003) [8] have identified nearly 10,000 landslides, which were triggered by the 1999 Chi–Chi earthquake (Mw 7.5), based on SPOT images. According to the findings, the distribution of landslides revealed a significant correlation with epicentral distance and the rock type. Furthermore, the geological features of deep-seated landslides and relatively smaller slides were described locally in Taiwan. Qi et al. (2010) [50] analyzed a spatial database of landslides which covers 11 countries severely damaged by the Wenchuan earthquake with an area of approximately 31,686 km^2. They pointed out that the distribution of landslides which are triggered by the earthquake have mainly depended on the distance to the causative faults and slope gradient. Basharat et al. (2013) [4] have analyzed the relationship between the distribution of the mass movements triggered by the 2005 Kashmir earthquake (Mw 7.6) with several parameters such as distance from an earthquake source (epicenter and fault), slope steepness, slope aspect, elevation and geological units. The results revealed that the mass movement concentration principally depends on the distance from the earthquake source. However, the topographic parameters and geological units play subsidiary roles in the distribution of mass movements.

2.2 Overview of Mid-Niigata Prefecture Earthquake

The location map of Mid-Niigata Prefecture Earthquake can be seen in **Figure 2.1**. The hypocenter of the main shock was located at a relatively shallow depth and the magnitude was 6.8. In addition to the main shock, it was followed by a number of large aftershocks and three of them had magnitudes larger than 6 (**Table 2.1**). Japan Meteorological Agency (JMA) scale recorded a seismic intensity of 7.0 in Kawaguchi and Ojiya, the maximum degree of this scale. **Figure 2.2** shows the epicenter location and the distribution of the seismic intensity following the JMA seismic intensity scale in Niigata Prefecture. Fault planes were estimated by the Geographical Survey Institute (2004a) [31] and Koketsu et al. (2004) [39] by using crustal deformation data and seismic waveform data observed by strong motion seismographs. Both studies proposed that the earthquake was caused by the slip off of the reverse fault. The estimated epicenter fault,

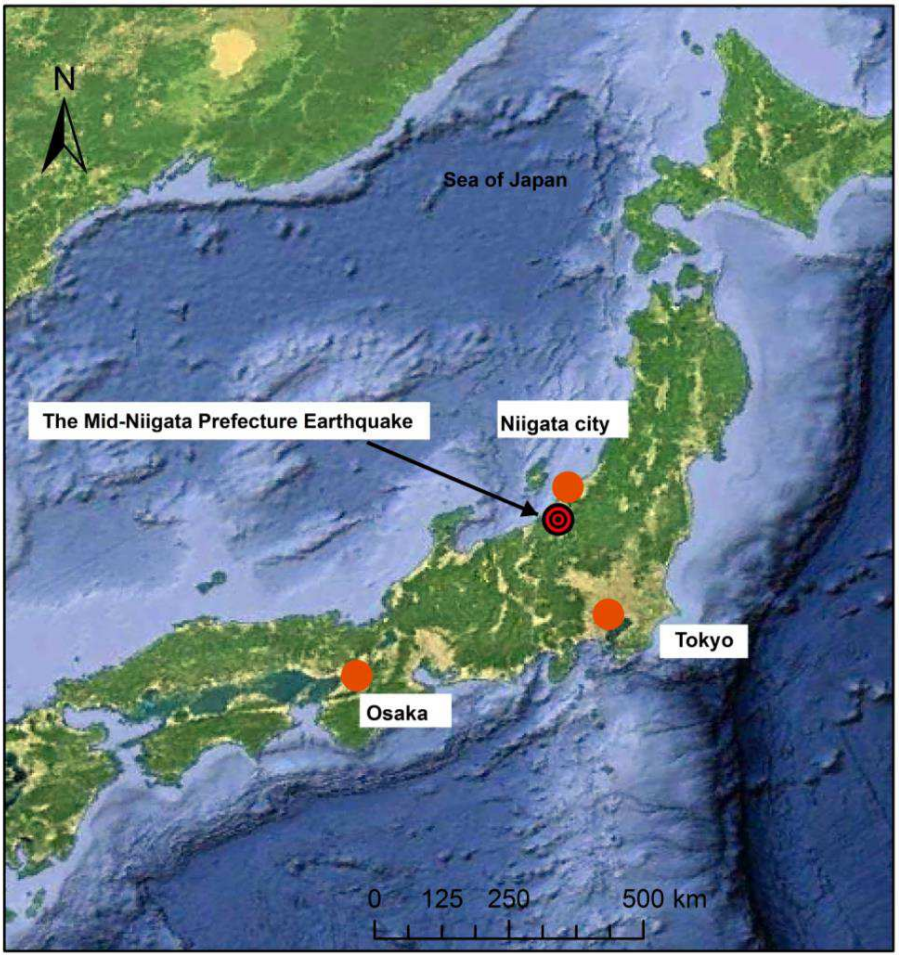

FIGURE 2.1: Location of the Mid-Niigata Prefecture earthquake

the crustal horizontal movement vector is shown in **Figure 2.3**. **Table 2.2** shows a summary of fault parameter.

2.3 Reviews of Previous Research

There are a number of studies that focused on the correlation of landslides associated with the 2004 Mid-Niigata Prefecture earthquake. Chigira and Yagi (2006) [9] recognized over 1000 landslides in areas underlain by Miocene-to Quaternary-aged sedimentary rocks. Among them, the most common type was shallow disrupted landslides on steep slopes, but deep landslides also occurred in many locations. Therefore detailed analysis was carried out for deep landslides via field investigation and by interpreting aerial photographs. It concluded that many landslides occurred because of reactivation of pre-existing landslides and mobilization of valley bottom sediments, probably due

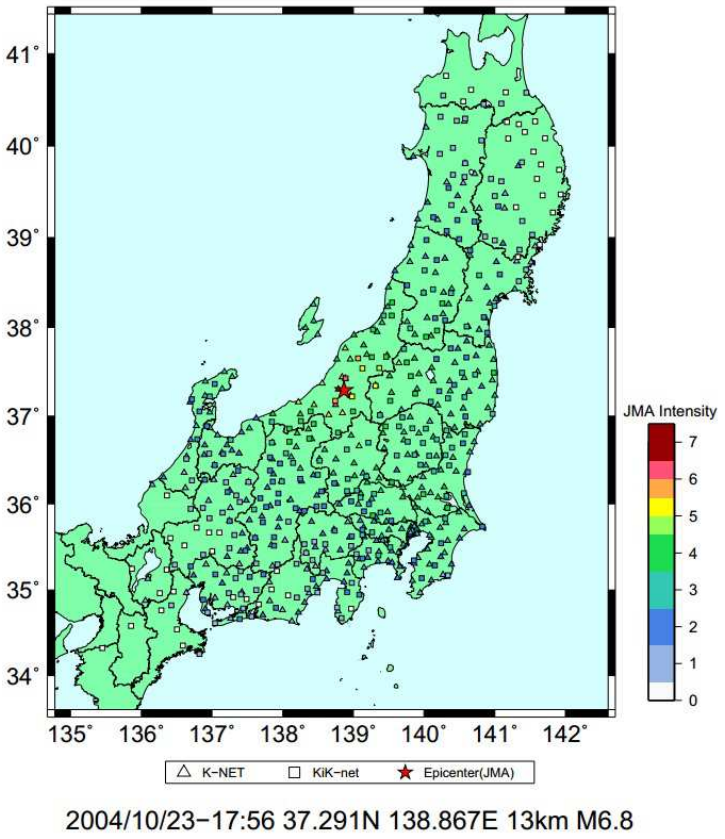

FIGURE 2.2: JMA Intensity Distribution Map (NIED 2004)

TABLE 2.1: The main shock and major aftershocks data

Year	Month	Date	Time occurred (JST)	Magnitude	Depth (km)
2004	Oct	23	17:56	6.8	13
2004	Oct	23	17:59	5.3	16
2004	Oct	23	18:03	6.3	9
2004	Oct	23	18:07	5.7	15
2004	Oct	23	18:11	6.0	12
2004	Oct	23	18:34	6.5	14
2004	Oct	23	18:36	5.1	7
2004	Oct	23	18:57	5.3	8
2004	Oct	23	19:36	5.3	11
2004	Oct	23	19:45	5.7	12
2004	Oct	24	19:48	4.4	14
2004	Oct	24	14:21	5.0	11
2004	Oct	25	0:28	5.3	10
2004	Oct	25	6:04	5.8	15
2004	Oct	27	10:40	6.1	12
2004	Nov	04	8:57	5.2	18
2004	Nov	08	11:15	5.9	<5
2004	Nov	10	3:43	5.3	5

TABLE 2.2: Summary of fault parameters

North latitude (°)	37.4
East longitude (°)	138.96
Length (km)	20.6
Width (km)	10.2
Distance to the ground surface from the upper end of surface fault = depth (km)	2.8
Angle strike (°)	210
Inclination angle (°)	53
Slip angle (°)	92
Slip (m)	1.82
Magnitude	6.8

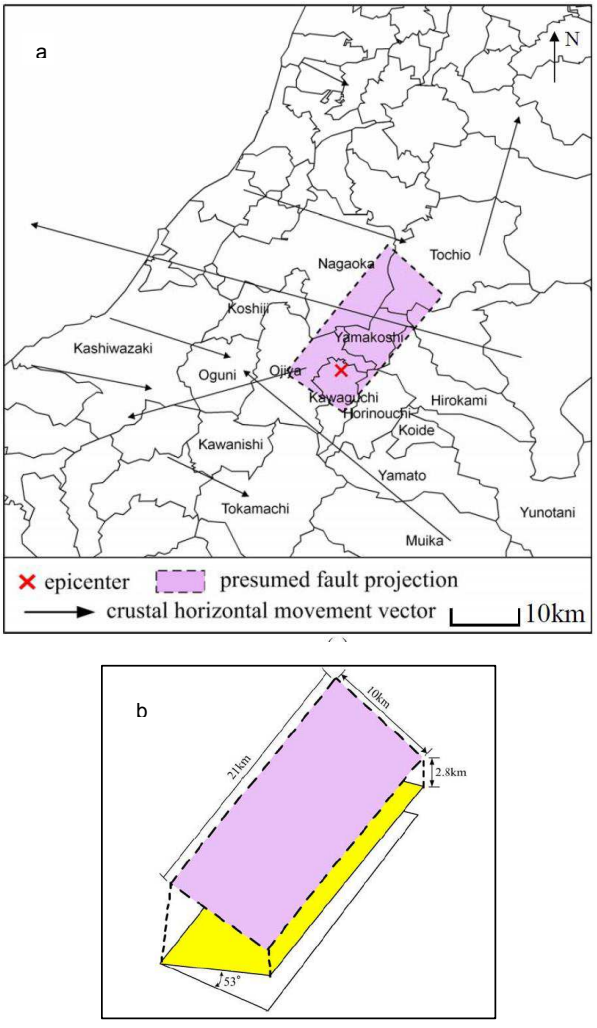

FIGURE 2.3: Estimated fault and the crustal horizontal movement vector [32]

to the saturation and partial liquefaction. Wang et al. (2007) [68] studied 1212 landslides with 641 that were reactivated from pre-existing landslides in a selected study area near the epicenter. landslides were statistically evaluated to clarify the correlation between geology, slope gradient, and earthquake motion. This found that landslides predominantly occurred on slopes in the 20°–35° range, that the maximum distance from the epicenter to the landslides was 18 km, that the Wanazu Formation had the most concentrated landslide activity, and the area affected by landslides was correlated with the earthquake magnitude. Sato et al. (2005) [55] digitally mapped 1553 landslides as polygons that included the source areas, travel paths, and accumulation areas. They found that landslides were concentrated more in the hanging wall than in the footwall. Kieffer et al. (2006) [37] concluded that a thrust fault caused more landslides in a wider area and showed that the greatest concentration of landslides is on the hanging wall side rather than the foot side.

Chapter 3

Description of study area and Data Preparation

3.1 Geographic Information System (GIS) Approaches

In recent years, GIS has been widely used in landslide hazard assessment (Carrara, 1991; [5] Aleotti and Chowdhury, 1999; [2] Dai et al., 2001; [14]). GIS provides strong functions for processing and analyzing the spatially distributed data. GIS has the ability to integrate qualitative as well as quantitative data and to collect, store, transform, evaluate and display a large amount of geographically referenced information needed for evaluation. Due to this excellent spatial data processing capacity, it has attracted great attention in natural disaster assessment (Carrara, 1983) [6]. Different types of data can be incorporated into GIS and represented as a map layer. Examples can include topography, zoning, landslides, geology, parcels, shopping centers, demographics, etc. (**Figure 3.1**). When these layers are placed on top of one another, undetected spatial trends and relationships often appear. This allows us to gain comprehensive knowledge about relevant characteristics of a location. Object or phenomena that can take place on or below the surface can be represented digitally using GIS tools. It provides different parameters of objects such as elevation, landslide, geology, slope morphology, and categorization based on attributes. Hence in this study, Arc GIS 9.3 is employed to analyze the correlation of landslides with geologic and geomorphologic factors.

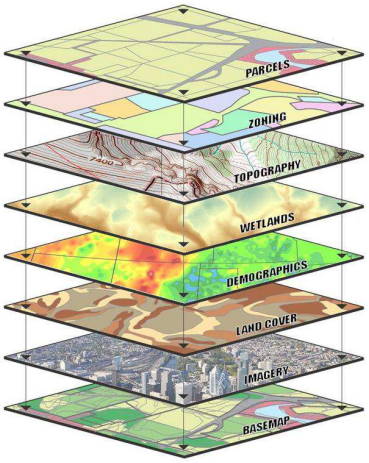

FIGURE 3.1: Examples for map layers

3.2 Geological Setting of the Study Area

The study area encapsulates Nagaoka city, Ojiya city, and Yamakoshi village. The epicentral area is located in the Higashiyama Hills and its adjacent alluvial plain, where the Shinano River flows from SW to NE but then reroutes to NW to N after merging with the Uono River. The Higashiyama Hills are northeast of the Shinano River (**Figure 3.2**). Yanagisawa et al. (1986) [77] and Kobayashi (1991) [38] summarized the geological outlines of the study area as follows. The Higashiyama Hills are underlain by a thick sequence of Miocene to lower Pleistocene sediments with many anticlines and synclines. The anticline and syncline axes from West to East are Higashiyama anticline, Konpira syncline, Toge anticline, Kajikane syncline, and Komatsuguru anticline, respectively (**Figure 3.3**). This area is tectonically very active with many active folds and active faults. Due to this anomalous tectonic and geologic context, many landslides have occurred previously. Hence pre-existing landslide deposits constitute a very common feature in the study area and they dramatically changed the geomorphic features.

3.3 Landslide Data

Figure 3.3 shows the distribution of the pre-existing landslide in the study area which is about $26703000m^2$. Probably these landslides were induced by historical earthquakes such as the 1828 Sanjo earthquake, the 1933 Ojiya earthquake, and the 1961 Nagaoka vicinity earthquake. A statistical analysis of landslide distributions was conducted for

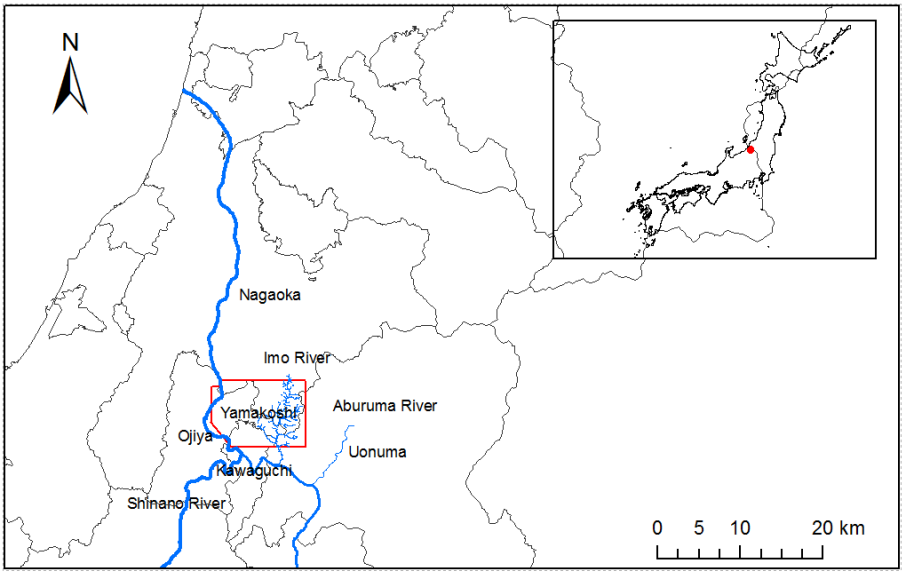

FIGURE 3.2: Index map of the study area

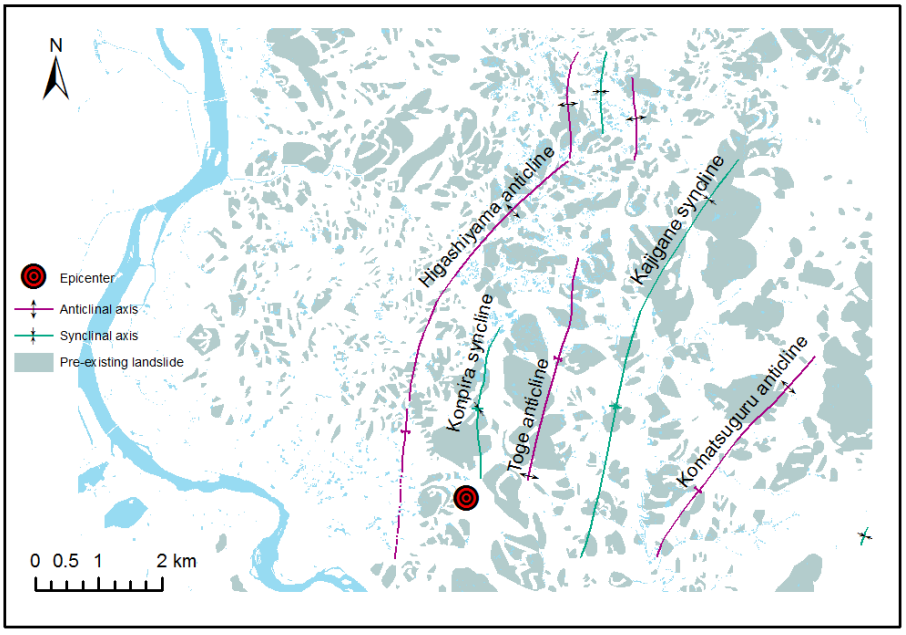

FIGURE 3.3: Pre-existing landslides, anticline, and syncline axes distribution

the landslides that were concentrated in the $86311904m^2$ study area as shown in **Figure 3.4**. The pre-existing landslide percentage was 30% of the study area. Hence during the statistical analysis, it is important to investigate the effect of pre-existing landslides for the occurrence of new landslides. After the earthquake, many research institutes, private sector companies, and universities carried out different types of investigation in the damaged area. As a results of that effort much hazard data became available. Inokuchi et al. (2008) [46] identified locations and areas of landslides by comparing aerial

TABLE 3.1: Summary of surface areas covered by earthquake-triggered landslides

Category	Number of landslides $\times(10^2)$	Total collapse area m^2 $(\times 10^6)$	Average collapse area m^2 $(\times 10^2)$
Deep slide	1.41	2.71	192.23
Shallow slide	6.09	1.25	20.58
Surficial slide	45.04	2.62	5.82

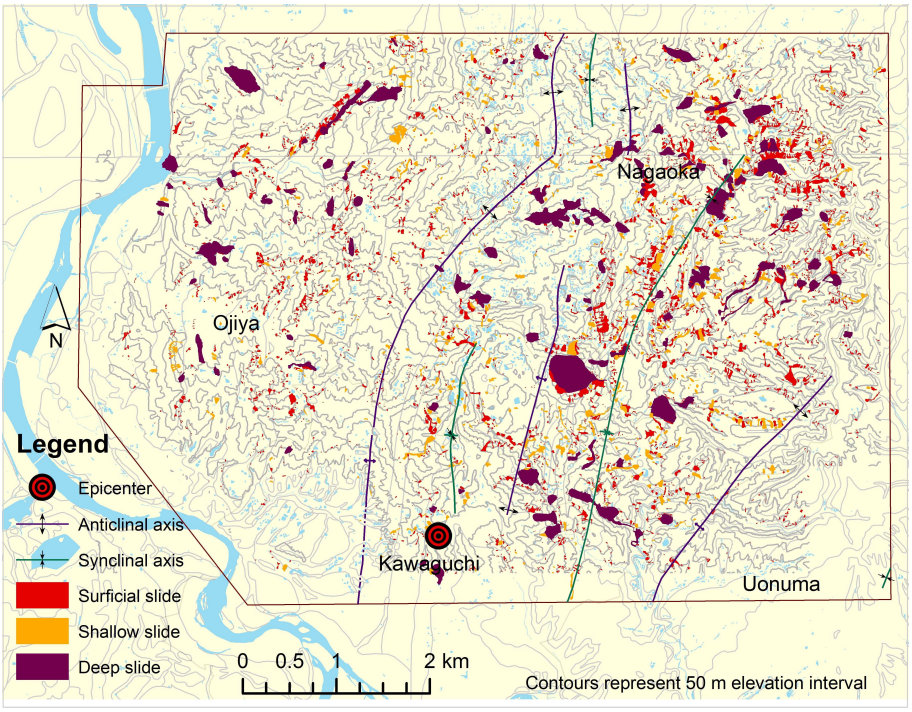

FIGURE 3.4: Distribution of earthquake-triggered landslides after the Mid-Niigata prefecture earthquake

photographs before and after the earthquake and verified them with field investigation. They have classified these landslides according to the depth of the slip surface, failure type, and materials of the moving body. The following three major landslide types were identified according to the depth of the slip surface: surficial slides (depth $\leq 1m$) (**Figure 3.5**), shallow slides (depth between 1 and 10 m) (**Figure 3.6**), and deep slides (depth $\geq 10m$) (**Figure 3.7**). These three types of landslides were further classified more specifically as rotational and translational. **Table 3.1** shows a statistical summary of the collapse area and the number of landslides within the study area. In the following thesis, 141 deep slides, 609 shallow slides, and 4504 surficial slides triggered by the 2004 Mid-Niigata Prefecture earthquake are analyzed in detail. The majority of landslides within the study area consist of surficial slides with a thickness of less than 1 m. Although the number of deep slides is relatively small, they contributed significantly to the total collapse area.

FIGURE 3.5: Surficial slide at Touge-guchi in Kawaguchi (photo by Suncoh Consultants Co.)

FIGURE 3.6: Shallow slide at Naranoki (photo by Ministry of Land, Infrastructure, Transport, and Tourism

FIGURE 3.7: Deep slide at Yuhugawa-haguroguchi in Yamakoshi (photo by Ministry of Land, Infrastructure, Transport, and Tourism)

3.4 Digital Elevation Model (DEM)

The Digital Elevation Model is a raster GIS layer. Raster GIS represents earth surface as a regular arrangement of locations. Each cell in the DEM has a value related to its elevation. DEM is used to calculate many useful derivatives of elevation, such as slope angle or slope aspect. In addition to that DEMs are allowed to create 3-D scenes or to create contours, which may be exported to CAD programs. The accuracy of the DEM is determined primarily by the resolution. **Figure 3.8** shows the 10m DEM of the study area.

Common uses of DEMs are as follows:

- Extraction terrain parameters
- Modeling of mass movement (for example avalanches and landslides)
- Terrain analyses in geomorphology
- Flight simulation
- Engineering and infrastructure design
- Rectification of aerial photography or satellite imagery
- Base mapping

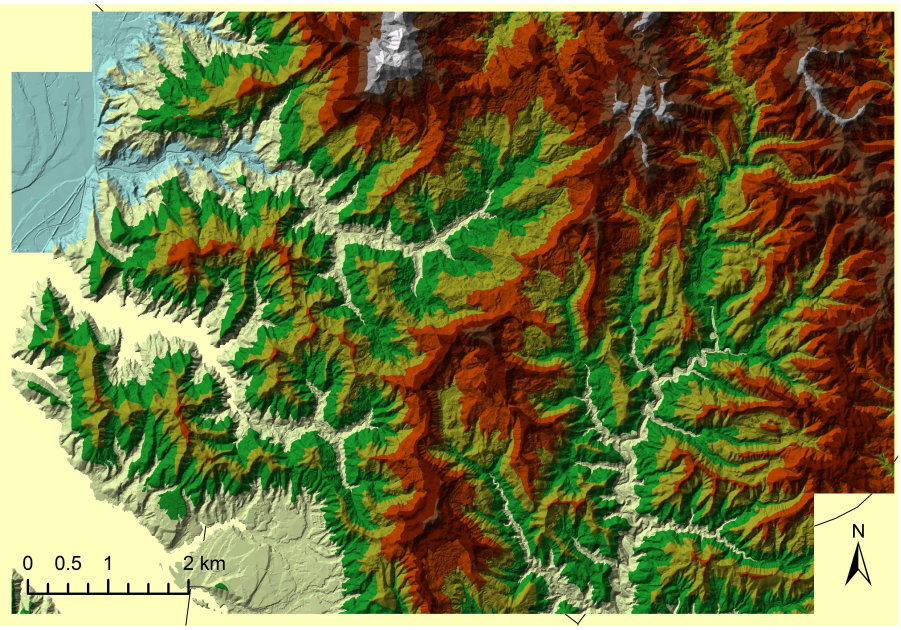

FIGURE 3.8: Digital Elevation Model (DEM) of Chuetsu region

a	*b*	*c*
d	*e*	*f*
g	*h*	*i*

FIGURE 3.9: Example of slope calculation

3.4.1 Slope Angle and Aspect

Slope calculates the steepness of the surface at any particular location. Slope value which means maximum rate of change between each cell and its neighbors can be calculated using the slope tool in the Arc GIS. In the output raster each cell has a particular slope value. The slope value is calculated according to its neighbour cells. Slope angle fits a plane to the z-values of 3×3 cell neighbourhood around the middle cell. The average maximum technique is used to calculate the slope value of this plane. Therefore the direction of the plane becomes the slope aspect of the middle cell or processing cell. **Figure 3.9** illustrates an example of the slope calculation. The cells are named as letters $'a'$ to $'i'$, with $'e'$ representing the cell for which the slope angle is being calculated (ESRI et al., 1998 [21]). **Figure 3.10** and **Figure 3.11** represent the slope and aspect calculation of the study area. The rate of change in the 'x' direction for cell

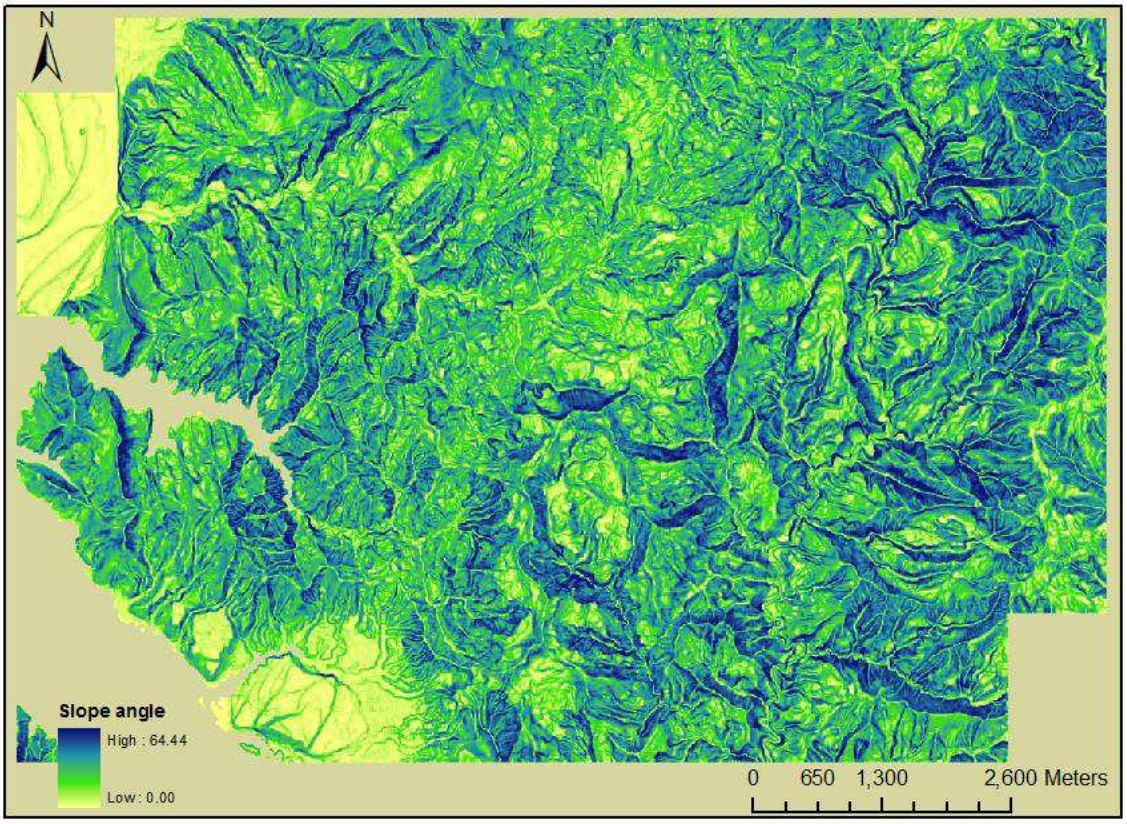

FIGURE 3.10: Distribution of inclination angle of the study area

$'e'$ is employing the following equation:

$$\frac{\mathrm{d}z}{\mathrm{d}x} = \frac{(c + 2f + i) - (a + 2d + g)}{(8 \times cellsize)} \tag{3.1}$$

The rate of change in the y direction for cell 'e' is calculated with the following equation:

$$\frac{\mathrm{d}z}{\mathrm{d}y} = \frac{(g + 2h + i) - (a + 2b + c)}{(8 \times cellsize)} \tag{3.2}$$

$$slope = tan^{-1}\sqrt{\left[\frac{\mathrm{d}z}{\mathrm{d}x}\right]^2 + \left[\frac{\mathrm{d}z}{\mathrm{d}y}\right]^2} \tag{3.3}$$

$$aspect = tan^{-1}\left(\frac{\text{- } \mathrm{d}z/\mathrm{d}y}{\mathrm{d}z/\mathrm{d}x}\right) \tag{3.4}$$

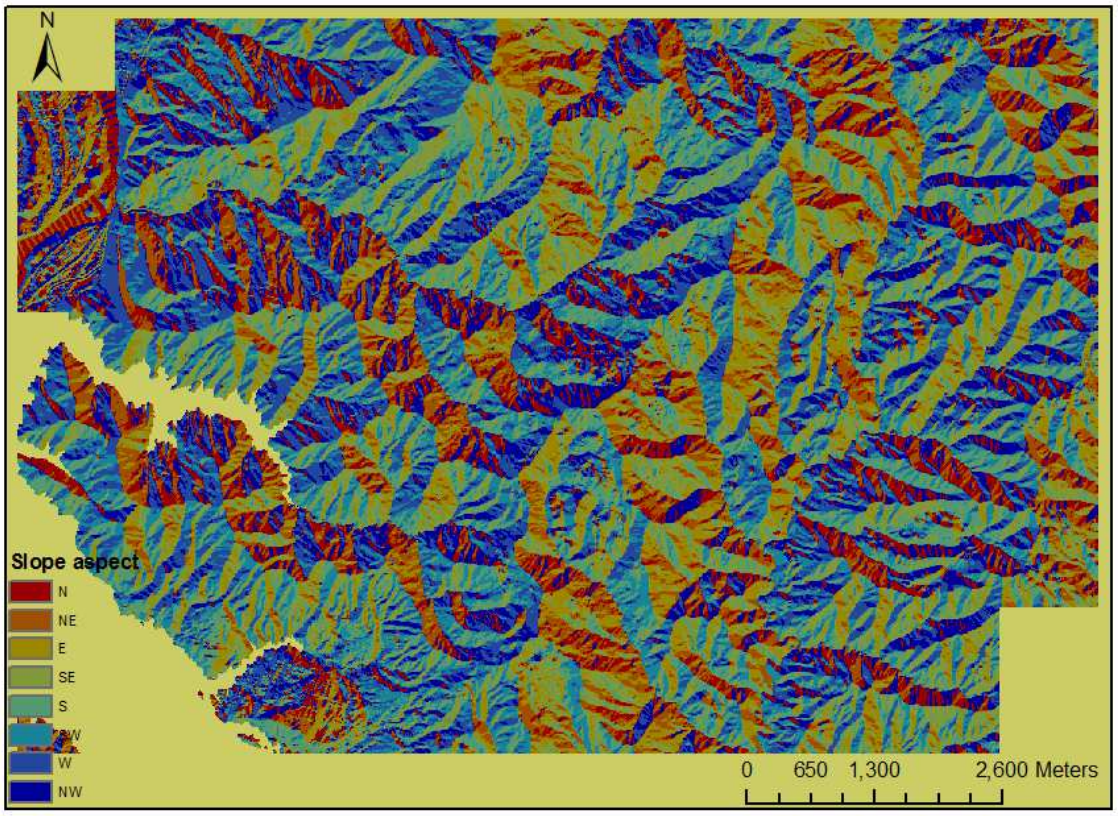

FIGURE 3.11: Distribution of slope aspect of the study area

3.5 Rock Types

Figure 3.12 shows the distribution of the rock types in the study area. The strata consist mainly of mudstone, igneous rock, sandstone, siltstone, and alternating beds of mudstone and sandstone. Mudstone and its interbedded sandstone are distributed in the center of the study area. Sandstone and siltstone are distributed in the west and east part of the study area.

3.6 River and Stream systems

A typhoon attacked Niigata prefecture three days prior to the earthquake and more than 150 mm of rainfall recorded during the 10 days before the earthquake struck. This large volume of precipitation is strong enough to saturate the soil or weathered rock, and the higher water table increased the ability for landslides to occur after strong ground motion due to the earthquake. The formation of the regional setting with Imo River and fish ponds of the study area increases the risk of the slope failure due to penetration

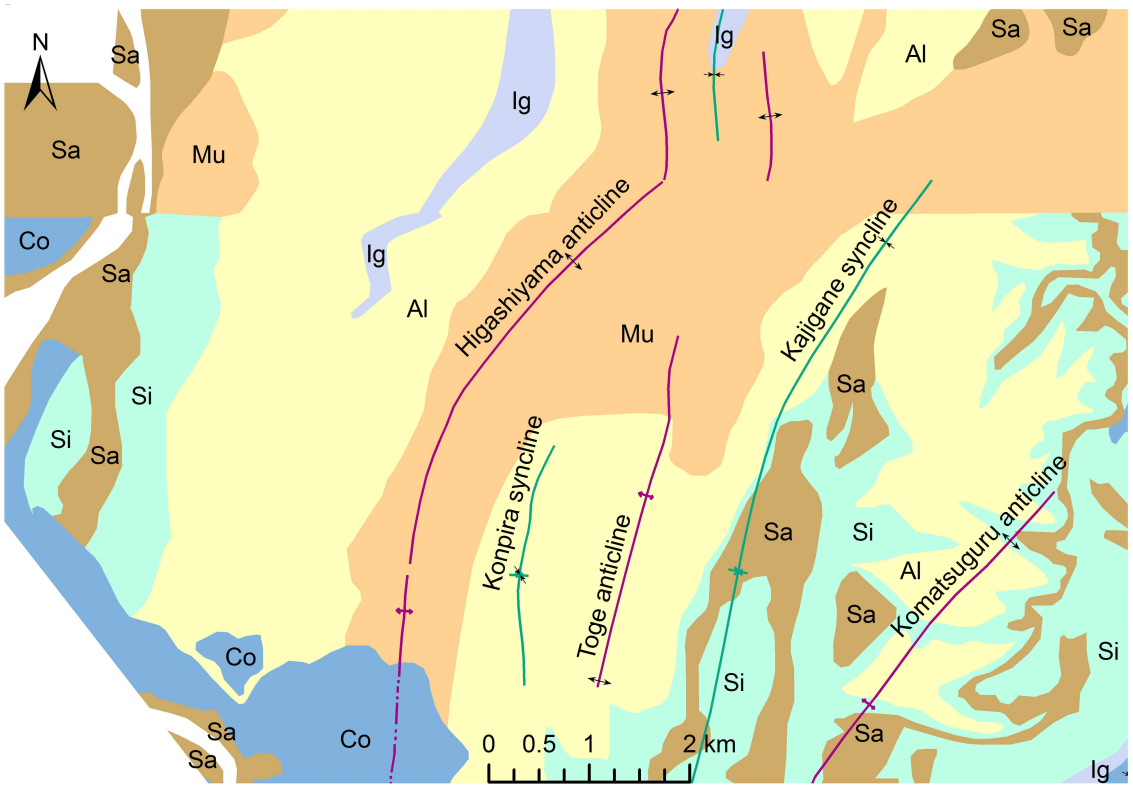

FIGURE 3.12: Geological outline of the study area. Ig igneous rock, Sa sandstone, Si siltstone, Al alternating beds of mudstone and sandstone, Mu mudstone, Co conglomerate

of surface water into soils or rocks. Many landslides occurred on the left bank of the Imo River which resulted in displacing a huge soil mass and blocked the river in the Yamakoshi village. In this study assumed that the ground water level is very high near rivers and ponds and low at the far end while calculating the effect of ground water level for occurrences of landslides. Distance from the rivers and ponds were considered as an indicator of ground water level.

3.7 Distance to Epicenter Fault line

The hypocenter of an earthquake is a point in the earth where a rupture starts to occur. The epicenter is a point on the ground surface directly above the hypocenter. **Figure 3.13** shows the relationship between the hypocenter, epicenter, fault plane, and rupture zone of an earthquake. Conceptually defined the epicenter fault fault line establishes the relationship between landslide occurrences with the earthquake source. **Figure 3.14** shows the landslide distribution with the epicenter fault line.

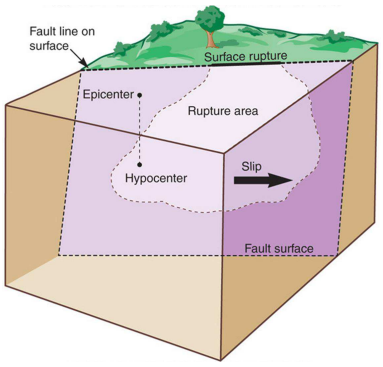

FIGURE 3.13: Definition of basic fault geometry including hypocenter and epicenter

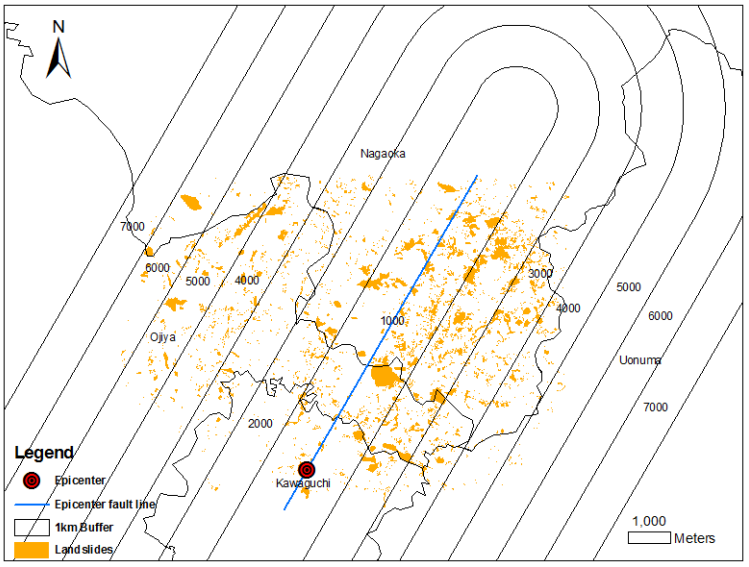

FIGURE 3.14: Landslide distributions with epicenter fault line

3.8 Overview of the Geological Structure

Natural beds and rocks are deposited as horizontal layers called strata. However, due to the gravity and other external forces, different layers may dip in any direction. Inclined bedding can identify as the simplest form of rock deformation. Even though the tilting is easy to visualize (**Figure 3.15**), describing the orientation of the inclination is challenging. Generally, beds can be inclined in any direction and in any amount from 0° to 90°. The term attitude explains the orientation in space of rock strata, however, it is not not enough evidence to conclude that beds are inclined. Each of the beds depicted in **Figure 3.15** is tilted about the same amount, although they are tilted in different directions meaning that they have different attitudes. Therefore it is important to have some indication of the direction of tilt and the amount of inclination. Geologists use two angular measurements to describe the orientation of a tilted layer of rock. The strike is

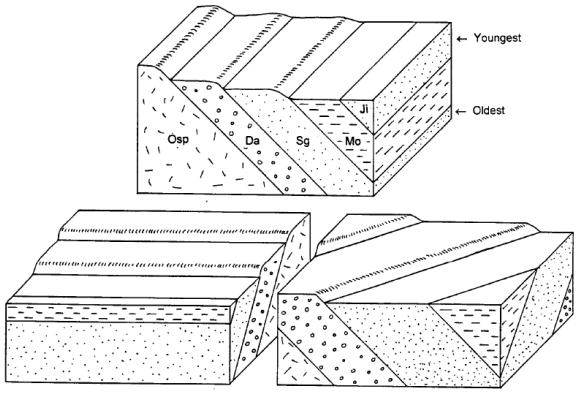

FIGURE 3.15: Inclined bedding, each tilted approximately the same amount, but in different directions

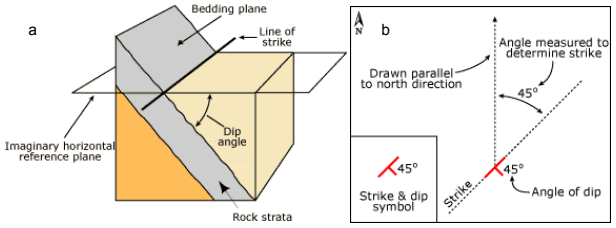

FIGURE 3.16: The strike-and dip-symbol and the determination of strike

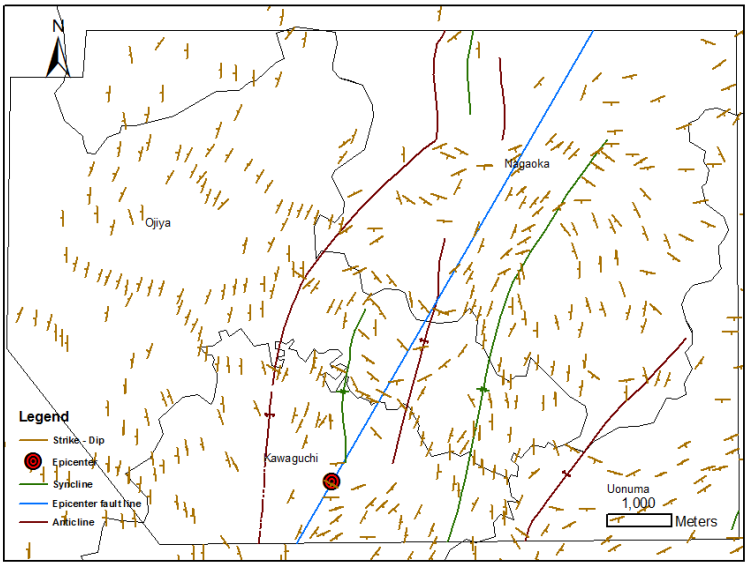

FIGURE 3.17: Geological structure of the study area

an imaginary horizontal line on a plane measured from the north that is usually reported as a measurement of compass direction. It is generally given in degrees. The dip is described as degrees measured downward from a horizontal plane (refer to **Figure 3.16** a). Geologists have represented the recorded dip data in the map using a line drawn according to the angle of the strike. A dip is indicated by a short line perpendicular to the strike in the direction of the dip. Taken together, the strike and dip of a tilted bed of rock describe its spatial orientation. Dip and strike are represented together with a "T" shaped mark on a map but it is not suitable to extract information for further analysis. Hence in this study, we introduced a three-dimensional gradient vector for attitude formation. The standard symbol for strike and dip is as follows (**Figure 3.16** b). **Figure 3.17** depicts the geological structure of the study area.

Chapter 4

Overview of the Preliminary Statistical Analysis of Landslide Distribution

4.1 Overview of the Preliminary Statistical Analysis

In this study, three main landslide types were analyzed to characterize their spatial distribution by correlating the landslide occurrence ratio (LOR) with the physical parameters that control the seismic stability of slopes. The LOR is defined as the ratio of the collapse area to the total area, where the collapse area is the surface area of landslide scars for a given class of a given predisposing factor and the total area is the total surface area for a given class of a given predisposing factor (Bandara and Ohtsuka, 2017 [3]) (Equation 4.1). These predisposing factors include the distance from the epicenter fault line, slope angle, distance from rivers and ponds, and rock type.

$$Landslide \quad Occurrence \quad Ratio = \frac{Landslide \quad collapse \quad area(m^2)}{Total \quad area(m^2)} \quad \times 100 \qquad (4.1)$$

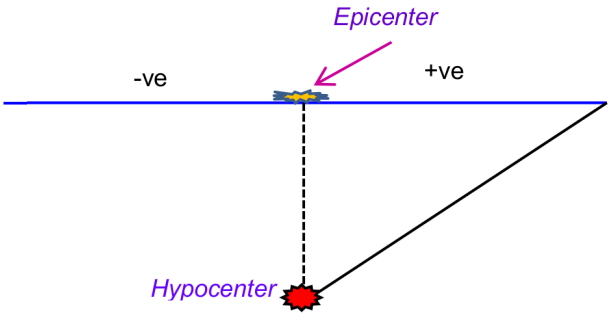

FIGURE 4.1: Distance from epicenter fault line

4.2 Collapse area and LOR in Viewpoint of Distance from Epicenter Fault Line

There are five different seismic parameters that can influence the earthquake-induced landslide (Xu et al., 2008b; [76] 2009b; [74] 2009c; [75]). (1) distance from coseismic fault ruptures (2) distance from the epicenter, (3) PGA, (4) seismic intensity, and (5) coseismic horizontal surface displacement, coseismic vertical surface displacement, and coseismic total surface displacement (De Michele et al., 2010; [16] Wang et al., 2011; [51] Shen et al., 2009 [60]). Therefore we analyzed the landslide distribution by considering distance from the epicenter fault line as a seismic parameter (**Figure 4.1**). In this preliminary study, we defined the negative distance zone and positive distance zone from the epicenter fault line.

Figure 4.2 shows the variation in surficial slide occurrence ratio with distance from epicenter fault line. It can be seen clearly that occurrence ratio of surficial slide is highest at the +0.5km from the epicenter fault line and drops off at +1.5km. Then after rising sharply during +2km, it steadily decreases again. However, variation of the occurrence ratio fluctuates in the negative zone. **Figure 4.3** presents the variation of shallow slide occurrence ratio with epicenter fault line. The results of the analysis indicate that the occurrence ratio of the shallow slide gradually decreases from the fault line to a maximum of 4.5km within the positive zone. However, the LOR does not follow the same movement in the negative distance zone. Variation of deep slide occurrence ratio with epicenter fault line can be seen in **Figure 4.4**. The LOR fluctuates throughout the entire area.

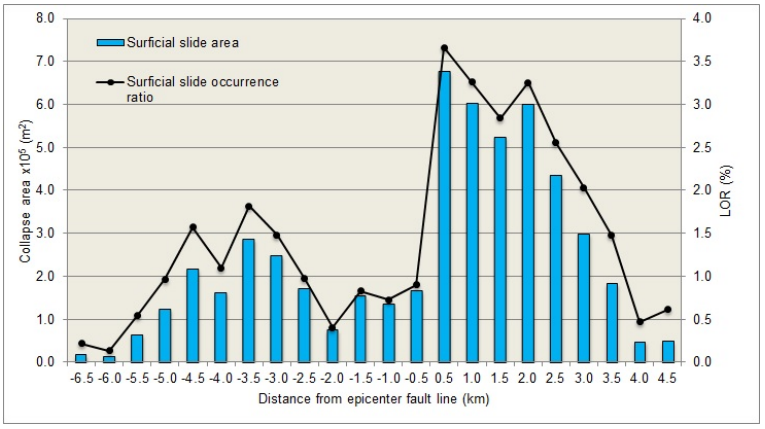

FIGURE 4.2: Surficial slide occurrence ratio according to distance from the epicenter fault line

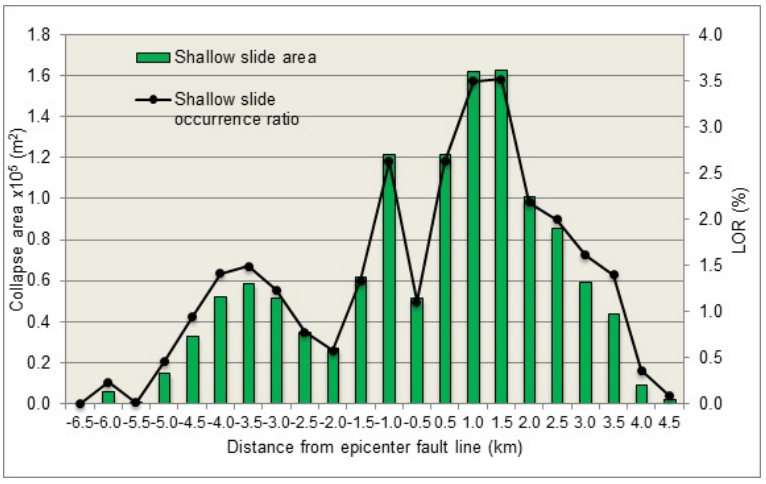

FIGURE 4.3: Shallow slide occurrence ratio according to distance from the epicenter fault line

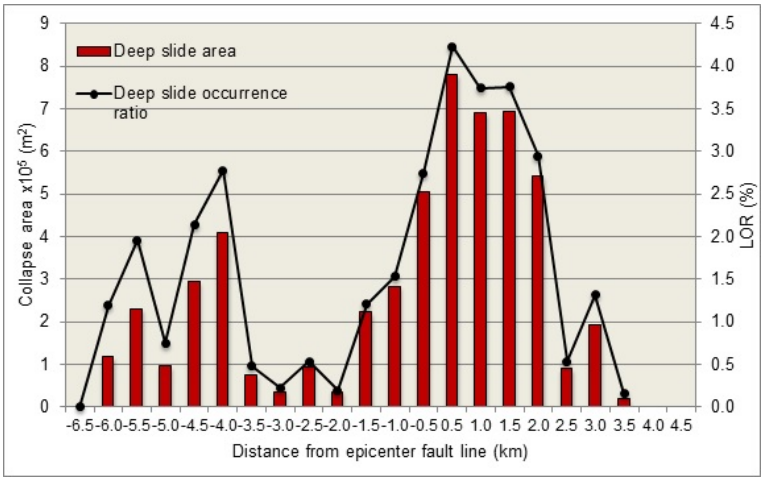

FIGURE 4.4: Deep slide occurrence ratio according to distance from the epicenter fault line

4.3 Collapse area and LOR in Viewpoint of Slope Angle

The mean slope angle was calculated for each landslide. Slope values are dependent on the resolution of their parent DEM. Most researchers have studied the slope maps derived from DEMs of different resolutions. Detailed studies were carried out by Chang and Tsai (1991) [7], Claessens et al. (2005) [11], Deng et al. (2007) [18] and Chow and Hodgson (2009) [10] for cell values between $8-80$, $10-100$, $5-480$, and $2-19m$, respectively. They show that mean slope is influenced by the cell size of the datasets used. Lee et al. (2004) [40] calculated the accuracy in landslide mapping with different spatial resolutions derived from a single-source DEM and concluded that at least 30m resolution of cell size is needed for landslide analysis. Zhang and Montgomery (1994) [79] evaluated the effects $4-, 10-, 30-$, and $90m$ resolution DEMs on the representation of the land surface and hydrologic simulations. This study documented that as grid size decreases, landscape features are more accurately resolved, but a faithful representation of a land surface by a DEM depends on both grid size and the accuracy and distribution of the original survey data from which the DEM was constructed. The study suggests that a grid size of $10m$ would suffice for many DEM-based applications of geomorphic and hydrologic modeling. Hence slope angle was extracted according to a digital elevation model (DEM) with $10 \times 10m$ resolution. As this study focused on small- to large-scale failures within a relatively wide area, this resolution is judged appropriate for extracting topographic features, assuming that the surficial slide which is less than 10 m does not have a significant effect on the analysis of LOR.

Figures 4.5, **4.6** and **4.7** show the relationship between landslide occurrence and the slope gradient categories. The surficial slide occurrence ratio increases with increasing slope gradient. This is because the shear stress in soil generally increases with the slope gradient. According to **Figure 4.6**, 66% of the collapse area of shallow slides are occupied by slopes between 25° and 35°. The shallow slide occurrence ratio is highest for the slope angle class of 30°. Almost all of the deep slides occurred at slope angles greater than 20°. The deep slide occurrence ratio increases with increasing slope gradient until a maximum is reached in the 25°–30° category (**Figure 4.7**) and then generally decreases with increasing slope gradient. The slope angle is an important factor determining the stability of a slope, but there are other factors. **Figure 4.8** shows surficial slide occurrence ratio with respect to distance from epicenter fault line and slope angle. As

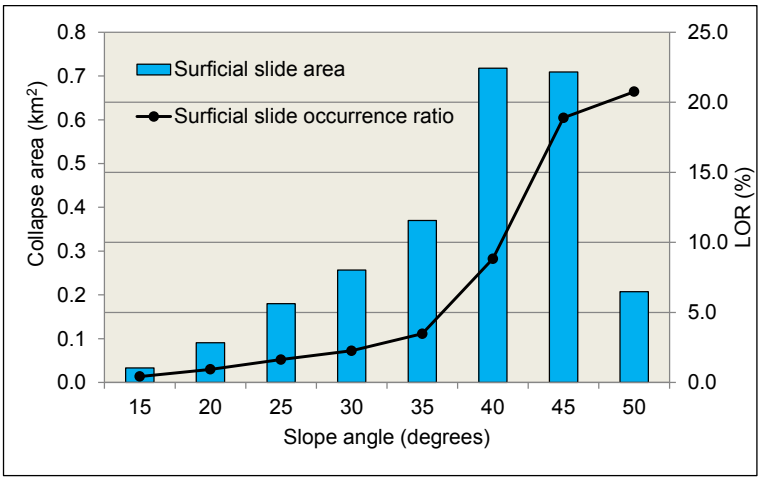

FIGURE 4.5: LOR and area of surficial slides according to slope gradient

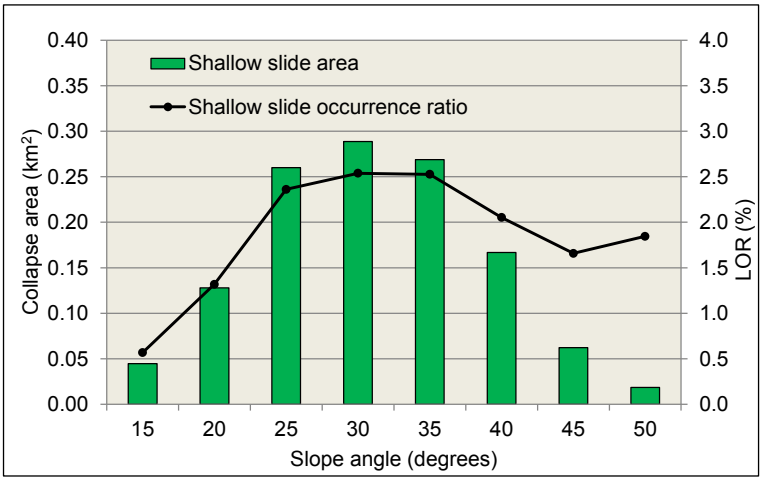

FIGURE 4.6: LOR and area of shallow slides according to slope gradient

shown in **Figure 4.8**, the surficial slide occurrence ratio is very low in the negative distance zone. This may be due to the higher ratio of gentle slope in that area. This result implies that the slope angle is strongly correlated with the earthquake induced surficial slide.

4.4 Collapse area and LOR in Viewpoint of Distance from Rivers and Ponds

Water is one of the most well-known causes of landslides in many parts of the world. Various landslide studies consider different impacts that water can have on the stability of slopes such as rising groundwater table and subsequent increasing pore water pressure, decreasing suction, seepage erosion, and subsequent infiltration (Johnson and Sitar,

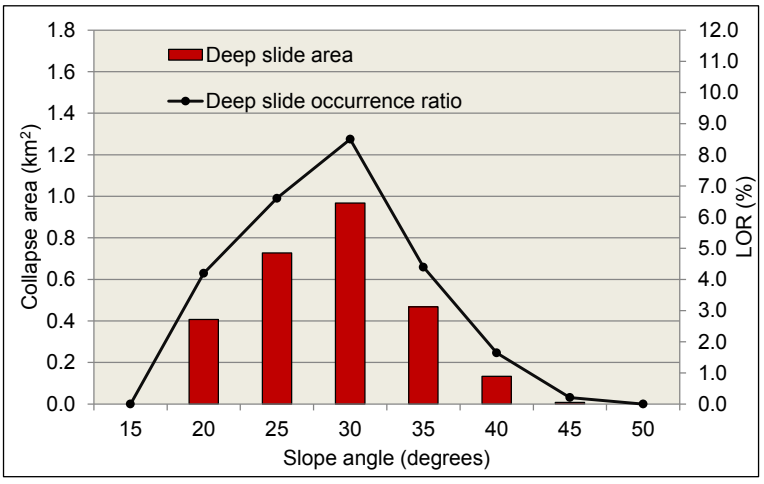

FIGURE 4.7: LOR and area of deep slides according to slope gradient

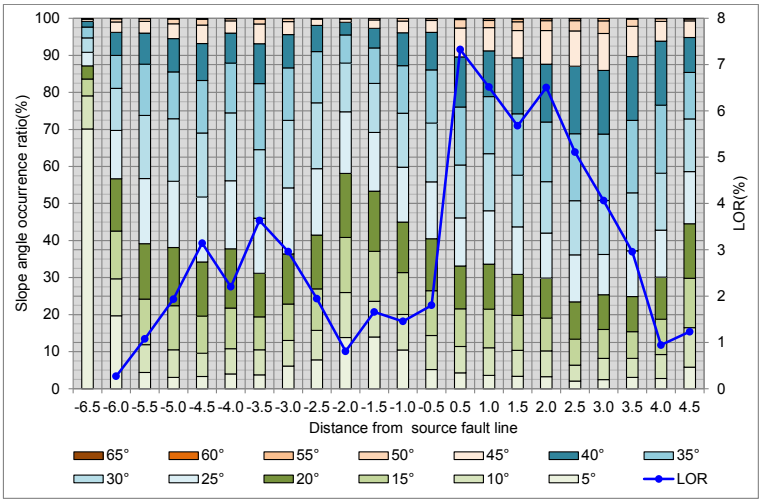

FIGURE 4.8: Total slope angle distribution and surficial slide occurrence ratio according to the distance from epicenter fault line

1990; [33] Leroueil et al., 1996; [41] Noverraz et al., 1998; [44] Van Asch et al., 1999 [64]). The study area study area features the Imo River where step farming paddy field and fish ponds formed the unique regional features. This regional setting increases the risk of landslide due to infiltration of surface water into soils or rocks. To investigate the effect of ground water level for occurrences of landslides we assumed ground water level was very high near rivers and ponds. Distance from rivers and ponds was considered as an indicator of ground water level. **Figure 4.9** shows the variation in surficial slide occurrence ratio with distance to rivers. The percentage share of surficial slide collapse area was 70.98% within a distance of 100m of rivers and ponds. **Figures 4.10** and **4.11** display the variation in the shallow slide and deep slide occurrence ratio with distance from rivers and ponds. It can be seen that the most of the landslide concentrated within

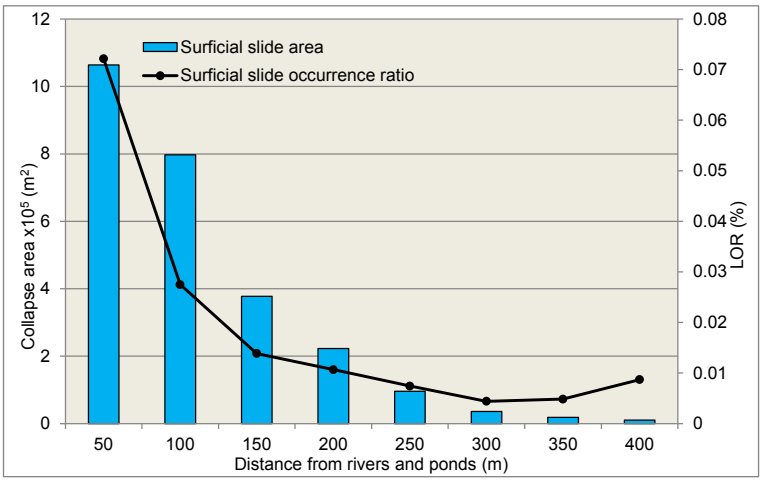

FIGURE 4.9: Surficial slide occurrence ratio and collapse area in viewpoint of distance from rivers and ponds

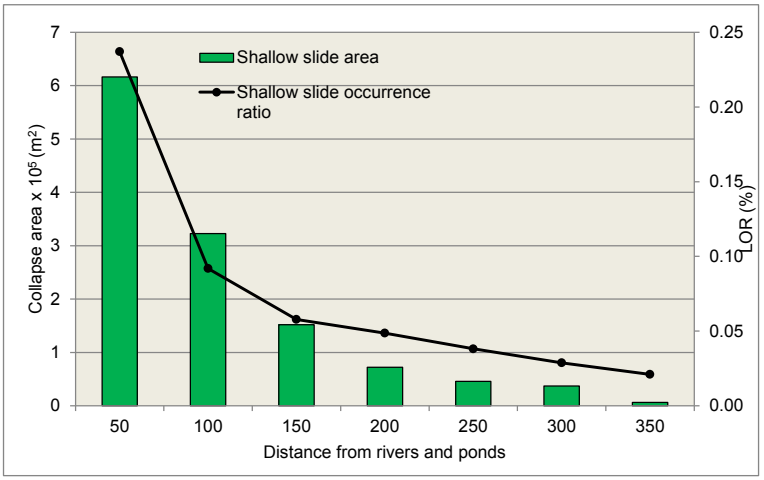

FIGURE 4.10: Shallow slide occurrence ratio and collapse area in viewpoint of distance from rivers and ponds

100m of the rivers.

4.5 Collapse area and LOR in Viewpoint of Rock Types

Rock types and geological structures can be identified as bases that control the overall strength of a rock mass. Therefore, rock type is one of the core parameters influencing slope stability. The study area is underlain by Miocene to Quaternary sedimentary rocks. It consists of mudstone, siltstone, sandstone, conglomerate, igneous rock, and alternating beds of mudstone (**Figure 3.12**). Distribution of surface area percentage of different rock types is provided in **Figure 4.12**. **Figure 4.13** represents deep slide occurrence ratio and area of each rock type and strata against the distance from the

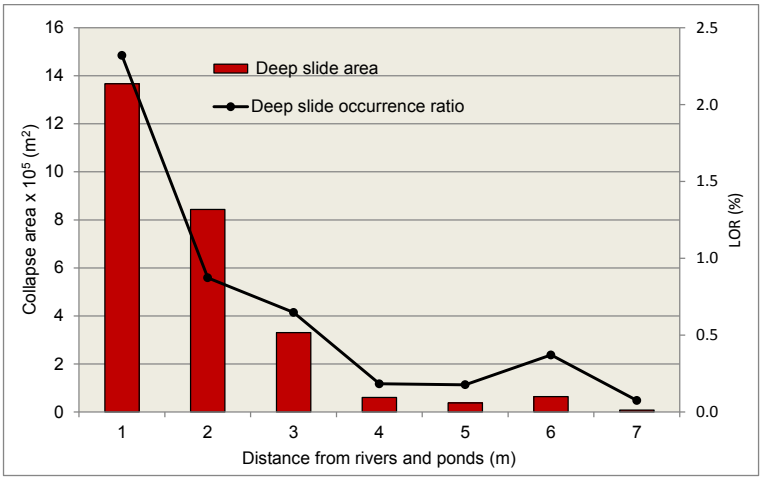

FIGURE 4.11: Deep slide occurrence ratio and collapse area in viewpoint of distance from rivers and ponds

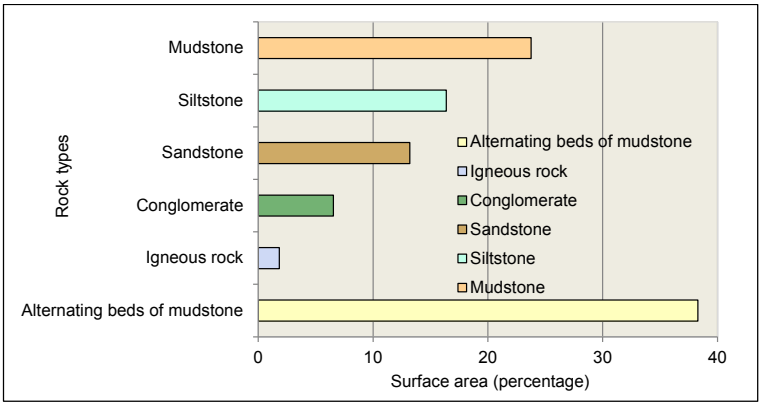

FIGURE 4.12: Distribution of surface area percentages of different rock types

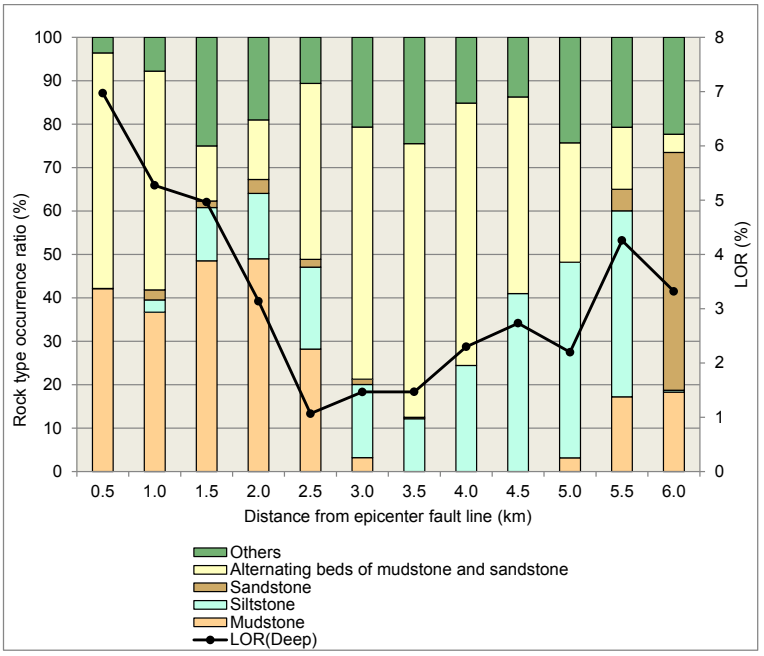

FIGURE 4.13: Landslide occurrence ratio and collapse area in viewpoint of geology types

epicenter fault line. It can be seen that the mudstone unit increases until 2.5 km from the epicenter fault line. It does not exist at a distance of 3.5 km to 5.0 km and only starts to appear again from 5.5 km. Furthermore, it can be seen that the area of siltstone increases from 3.5 km to 5.5km. This arrangement is inadequate for offering a better conclusion regarding influence of rock types on landslide distribution, and therefore more comprehensive analysis is carried out in **Chapter 5**.

Chapter 5

Spatial Distribution of Landslides Induced by the 2004 Mid-Niigata Prefecture Earthquake, Japan

5.1 Overview of the Bedding Attitude Prediction

Geometric relationships between topography and geologic structure can be influenced by subsurface drainage and mass wasting (Freeze and Cherry, 1979; [23] Selby, 1993 [59]). This is particularly evident where the geologic structure is characterized by penetrative discontinuities, such as sedimentary bedding or schistosity (Sander, 1970; [54] Cruden, 1989 [13]). Bedding planes have been identified as factors controlling the type, abundance, and pattern of landslides (Fookes and Wilson 1966; [22] Zaruba and Mencl, 1969 [78]). Mathematical relationships and statistical approaches between the landslide distribution and their causative factors are prepared on the basis of polygons as mapping units. However, attitudes of geological structures are marked usually as linear or point measurements on feature maps (**Figure 5.1**). Dip and strike are represented together with a T-shaped mark on a map. In addition to that anticline (up folded or arched rock layers) and syncline (down folds or troughs of rock layers) are also marked as a line (**Figure 5.2**). **Figure 5.3** shows strike and dip trends of strata associated with a plunging anticline and a plunging syncline. This study proposes a GIS-based method

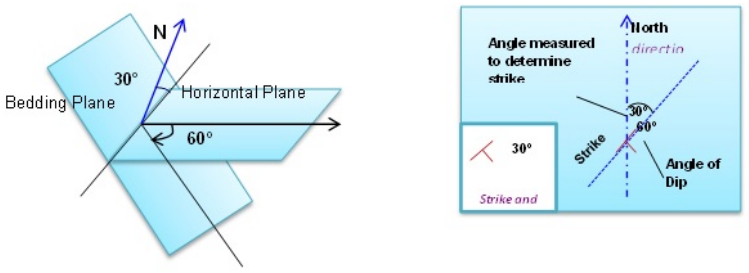

FIGURE 5.1: Strike and dip of an inclined bed

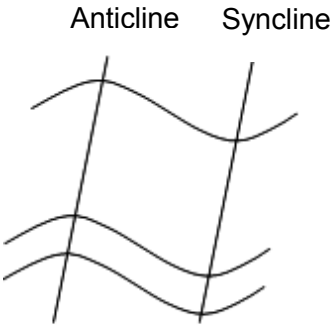

FIGURE 5.2: Anticline and syncline representation on factor map

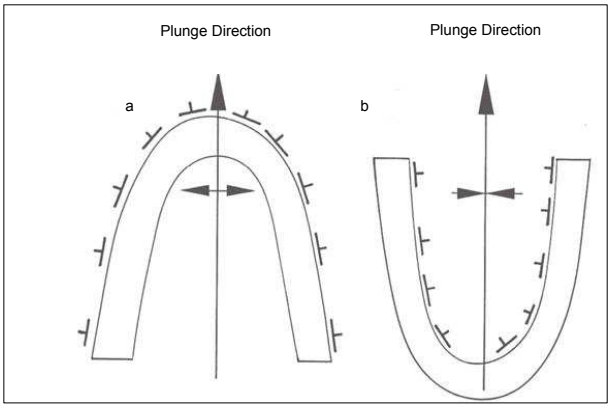

FIGURE 5.3: Strike and dip trends of strata associated with (a) plunging anticline and (b) plunging syncline

to estimate geometric alignment between topography and the orientation of geologic bedding planes.

5.1.1 Bedding Interpolation Procedure

The different models are considered for predicting the structure of a random point. In general, different models have different characteristics, hence applying the appropriate method or integrating several methods for the optimal prediction of the structure is

TABLE 5.1: Conditioning factors and significance of each model

Conditioning factors	Significance
Positional relationship from observation points to any point	Direction and number of observation points for prediction
3D prediction	Expression by vector
Distance relationship from the observation points to any point	Introduced weighting function
Anticline and syncline axis	Anticline and syncline axis split in to many segment (considered as point data)

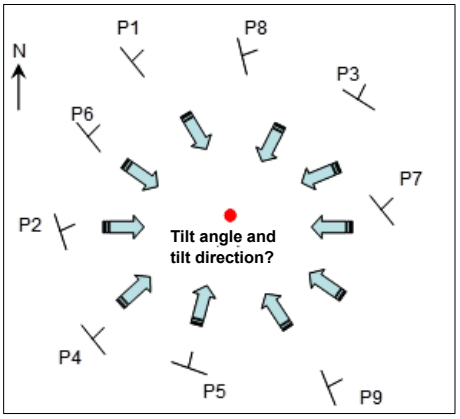

FIGURE 5.4: Concept of the geological structure prediction of a random point

important. **Table 5.1** shows the conditioning factors and significance of each method. The basic concept of the geological structure prediction of an arbitrary point can be seen in **Figure 5.4**. To evaluate the performance of the model, the predicted dip and dip direction results were evaluated statistically in comparison with field data (e.g. compared to strike and dip measurements as they appear on a conventional geological map). Sampling points (596) were extracted at locations that coincide with field dip and strike calculation.

5.1.1.1 Direction and Number of Observations

There are two different models studied according to direction and number of the measured points around the prediction location. Those methods considered 4 points and 8 points around prediction location that reflect the 4 directions and 8 directions. **Figure 5.5** shows the example calculation and selecting the appropriate points to be used in the analysis. In the example shown here, the measured values surrounding the prediction location have been divided into 8 divisions and 4 divisions. From each directions or divisions one measured value is considered which is closest to the prediction location.

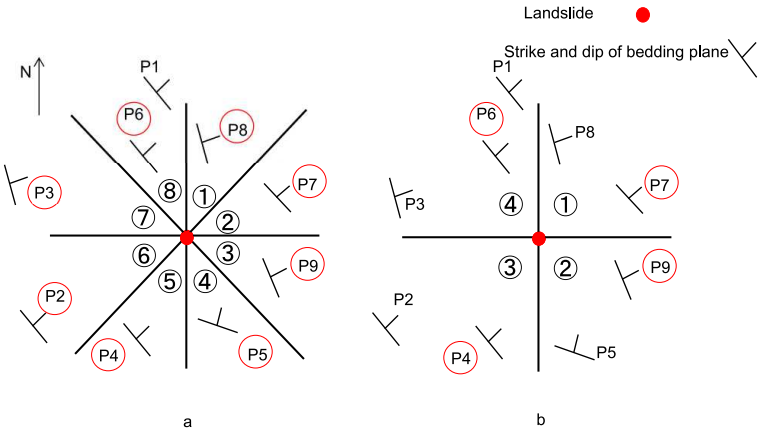

FIGURE 5.5: Illustration of search neighborhood. a Eight-sector search area. b Four-sector search area landslides search area Landslides

TABLE 5.2: Comparison of the coefficients of correlation between the true and predicted values of dip direction and dip angle considering the direction

		4 division	8 division
Correlation coefficient between the true value and predicted value	ϕ	0.777	0.782
	θ	0.812	0.792

According to that phenomenon the point highlighted in each sector such as P8, P7, P9, P5, P4, P2, P3, and P6 accounted for the calculation (**Figure 5.5** (a)). Comparing the coefficients of the correlation between the true and predicted values of dip direction and dip angle considering the direction can be seen in the **Table 5.2**. Even though the ϕ is highly correlated at 8 division prediction θ is highly correlated at 4 division prediction. According to the results, it does not increase the correlation when increasing the number of the division or direction, hence the 4 division method adopted in the prediction is chosen due to less computational time being required.

5.1.1.2 Three Dimensional Vector Representation of Attitude

The strike and dip directions are angular values in the range 0°–360° and 0°–90°, respectively. As an example, for two beddings dipping to the NNE (N20) and to the NNW (N340), averaging of the two strike values will provide a completely inaccurate result (N180, instead of N360). Therefore the polarity of the bedding plane must be accounted for when predicting the bedding measurements. To accomplish this task, a single bedding measurement is treated by an outward unit vector, and measurements are combined using analytic geometry (Shiono 2008) [61]. Equation 5.1 gives the three

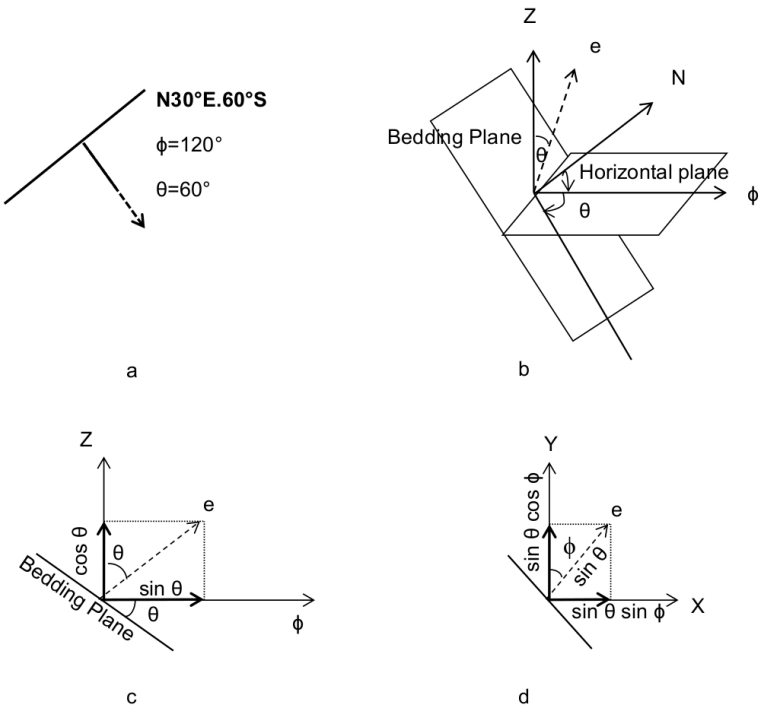

FIGURE 5.6: Vector representation of bedding plane. (a) Relationship between dip, strike, and θ, ϕ . (b) Relationship between θ, ϕ, and component of the unit vector. (c) Relationship between θ, ϕ, and Z component. (d) Relationship between θ, ϕ, and X, Y

components of the unit vectors in the bedding plane (**Figure 5.6**), where ϕ is the dip direction and θ is the dip angle of the bedding plane.

$$\begin{aligned} e_x &= sin\theta.sin\phi \\ e_y &= sin\theta.cos\phi \\ e_z &= cos\theta \end{aligned} \tag{5.1}$$

5.1.1.3 Inverse Distance Weighted Interpolation (IDW)

The effect of the distance between a predictive point and measured point is investigated using Inverse Distance Weighted (IDW) interpolation. We assumed that things that are close to one another are more alike than those that are farther apart. To predict a value for any unmeasured location, IDW uses the measured values surrounding the prediction point. It is calculated according to Equation 5.2. The measured values closest to the

TABLE 5.3: Comparison of the coefficients of correlation between the true and predicted values of strike and tilt in a different weighting function

$Z = (1/r^B)$				
	B	0	1	2
Correlation coefficient	Strike	0.783	0.798	0.803
	Tilt	0.794	0.802	0.788
The average value of the inner product		0.962	0.967	0.965

prediction location have more influence on the predicted value than those farther away. IDW assumes that each measured value has a local effect that decreases with distance. It gives greater weights to points closest to the prediction location, and the weights diminish as a function of distance. This study we have compared the correlation of each different weighting pattern function. **Table 5.3** represents the comparison of the true value and predicted value due to the difference in weighting function.

$$\phi = \frac{\sum_{i=1}^{n} \frac{\phi_i}{(r_i)^B}}{\sum_{i=1}^{n} \frac{1}{(r_i)^B}}, \qquad \theta = \frac{\sum_{i=1}^{n} \frac{\theta_i}{(r_i)^B}}{\sum_{i=1}^{n} \frac{1}{(r_i)^B}} \tag{5.2}$$

where r_1^B.....r_n^B is the distance from n data points to the power of B of the point estimated,

ϕ, θ = is the estimated value, and

ϕ_i, θ_i is the observed value at location i.

5.1.1.4 Anticline and Syncline Consideration

Synclinal and anticlinal axes were considered for the prediction of the dip and strike and were digitally represented as polylines. Polylines were converted into point data with intervals of 100, 500, or 1000 m, and we assumed that the vector components of the selected points were $\boldsymbol{e}$ (0,0,1). **Table 5.4** shows the average inner product of the true and predicted values of the dip direction and dip angle considering anticlinal and synclinal axes.

TABLE 5.4: Comparison of the coefficients of correlation between the true and predicted values of dip direction and dip angle considering the synclinal and anticlinal axes

Interval (m)	without	1000	500	100
Average inner product	0.9671	0.9696	0.9699	0.9691
Number	596	596	594	594

5.1.2 Cross-Validation

The spatially distributed geometrical information is used to calculate the magnitude of the unit vector; the dip angle of the bedding plane, θ ; and the dip direction of the bedding plane, ϕ. To analyze the performance of the model, the predicted dip and dip direction results were evaluated statistically in comparison with field data (e.g., the sampling points were extracted at locations that coincide with field dip and strike measurements as they appear on a conventional map). The correlation was analyzed by considering the inner product of the true values and predicted values of the dip direction and dip angle, because the dip direction and dip angle are vectors. Inner products that are closer to 1 indicate higher correlation. According to **Table 5.4** 500m interval points show the highest correlations since the average inner product is closer to 1. Hence, these points on the anticlinal and synclinal axes are considered for the prediction of the dip and strike. From **Table 5.3**, B=0, it can be seen that the correlation is lowest without considering the distance from the observation point. According to the results the correlation is highest when weighting function $B = 1$. Hence that weighting function is considered for the prediction.

5.1.3 Slope Types

On the basis of the geometrical relationship between the orientation of the bedding planes and the geometry of the slopes, slopes can be classified as follows (**Figure 5.7**): (a) dip slope (cataclinal), where the bedding plane dips in the same direction as the slope, (b) reverse dip slope (anaclinal), where the bed dips in the direction opposite to the slope, and (c) horizontal dip slope (orthoclinal), where the azimuth of the dip direction is perpendicular to the azimuth of the slope direction (Grelle et al., 2011) [25]. The difference between bedding and terrain orientations is calculated for classification of the slope types. The relative inclination γ is a function of the topographic slope, aspect, bedding dip direction, and inclination. For a bedding inclination θ and dip direction ϕ,

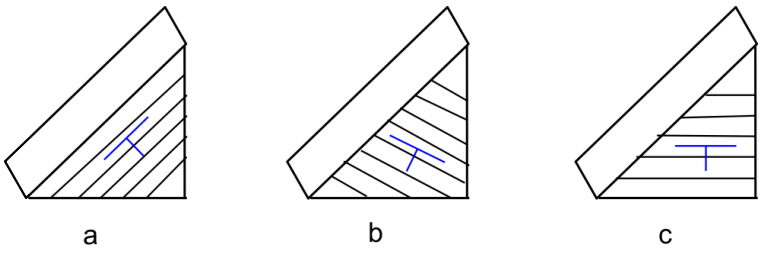

FIGURE 5.7: Bedding slope relationship. a Dip slope. b Reverse dip slope. c Horizontal dip slope

the strike μ ($0\ ^\circ \leq \mu \leq 180^\circ$) and dip angle δ ($0^\circ \leq \delta \leq 90^\circ$) of the landslide slope can be calculated as

$$\begin{aligned} \mu &= \phi - 90^\circ \\ \delta &= \theta \end{aligned} \tag{5.3}$$

The mean slope angle and mean slope directions for each landslide were calculated using the DEM. If the terrain orientation of the landslide is η, the difference between the bedding orientation and terrain orientation (α) and apparent dip (β) can be calculated as

$$\alpha = \mu - \eta \tag{5.4}$$

$$\beta = -tan^{-1}(tan\delta.sin\alpha) \tag{5.5}$$

The relative inclination γ is obtained from the apparent dip as

$$\begin{aligned} if \beta \geq 0^\circ, \qquad \gamma &= \beta \\ \beta < 0^\circ, \qquad \gamma &= 180^\circ + \beta \end{aligned} \tag{5.6}$$

The value of the relative inclination γ can be used to separate slopes categorized as having different bedding geometries (Suzuki T 2000):

$$\begin{aligned} 0^\circ \leq \gamma < 10^\circ &\qquad \text{horizontal dip} \\ 10^\circ \leq \gamma < 87.5^\circ &\qquad \text{dip} \\ 87.5^\circ \leq \gamma < 97.5^\circ &\qquad \text{vertical dip} \\ 97.5^\circ \leq \gamma < 180^\circ &\qquad \text{reverse dip} \end{aligned} \tag{5.7}$$

5.2 Variation of Landslide Occurrence Ratio with Slope Structure

The proposed methodological procedure makes it possible to predict the bedding attitude of a random point. The purpose of this procedure, basically, is to identify three types of a slope, specifically a dip slope, reverse dip slope, and horizontal slope. The LOR and collapse area according to the bedding orientation are shown in **Figure 5.8**. The occurrence ratio for deep slides is greater for dip slopes than for other configurations. However, the surficial slide occurrence ratio is higher for horizontal dip slopes, but the difference between dip slopes and horizontal dip slopes is very small. In addition, the shallow slide occurrence ratio is more or less equal for all the slope types. This result shows that shallow slides occur independently of the macroscopic structure of the slope. As pre-existing landslides have greatly changed the slope morphology and strength properties of the intact ground, the effect of pre-existing landslides on the LOR is further investigated in **Figure 5.9**. The figure shows that deep slides are apt to occur for dip slopes, but the occurrence ratio of pre-existing landslides is also higher. Further, the total sliding area of pre-existing landslides is somewhat greater than that of dip slopes. However, the occurrence ratios of surficial and shallow slides are more or less equal regardless of the slope. This result reflects the fact that the macroscopic slope structure does not significantly affect the occurrence of shallow slides and surficial slides when the effects of pre-existing landslides are considered. Deep slides are influenced mainly by whether the bedding plane is parallel to the slope.

5.3 Variation of Landslide Occurrence Ratio with Slope Aspect

The study area consists of many anticlinal and synclinal axes, which are almost parallel to the fault direction. Our analysis considers whether the fault direction affects the stability of the slopes. The slope aspect may also affect landsliding because it is related to factors such as the directional peak ground acceleration (Dai et al., 2011) [15]. The LORs and collapse area for slope aspect classes are presented in **Figure 5.10**, **Figure 5.11**, and **Figure 5.12** with the fault direction, which is represented by the line through the radar

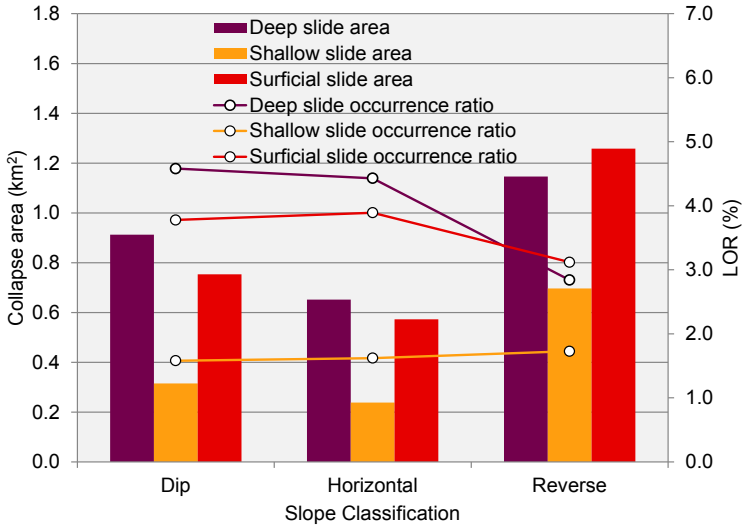

FIGURE 5.8: Occurrence ratio and collapse area according to slope morphology and slope classification (see **Figure 5.7**)

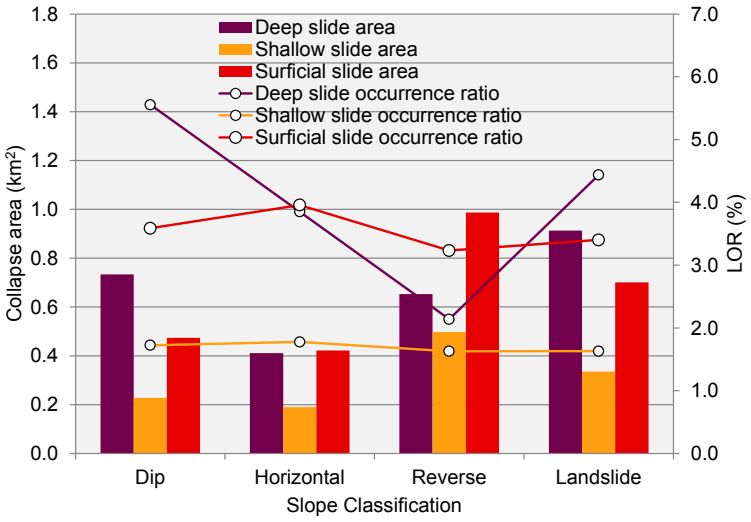

FIGURE 5.9: Occurrence ratio and collapse area according to slope morphology, pre-existing landslide deposits, and slope classification (see **Figure 5.7**)

charts. Surficial slides occurred mainly on the south, southwest, and southeast facing slopes (**Figure 5.10**). The relationship between the shallow slide occurrence ratio and the slope aspect is shown in **Figure 5.11**. The occurrence ratio of shallow slides is highest on the southwest facing slopes. Although the sliding directions of shallow and surficial slides are relatively scattered, the dominant direction is still south to southwest. Surficial and shallow slides that face approximately parallel to the fault direction are more prone to failure. However, this trend is moderate and the change in LOR with the direction of the slope is continuous. In contrast, **Figure 5.12** shows that the occurrence ratio of deep slides is highest for east facing slopes. This result indicates that the

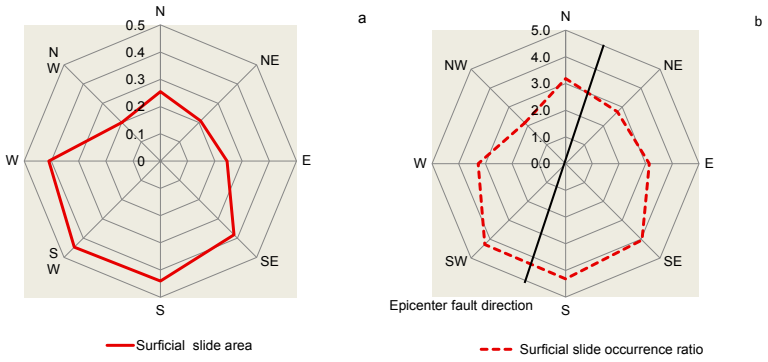

FIGURE 5.10: Surficial slide LOR and collapse area according to slope aspect

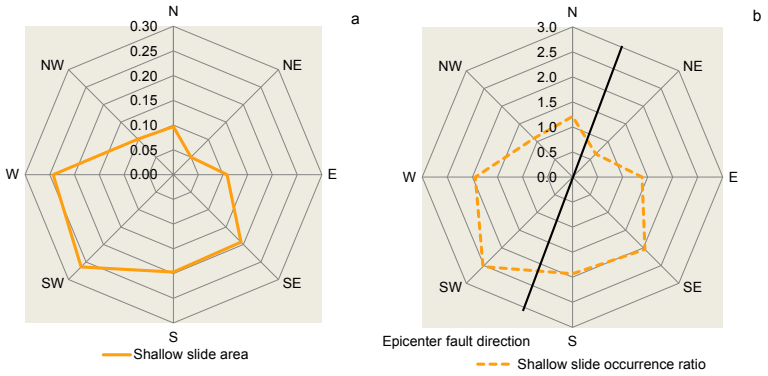

FIGURE 5.11: Shallow slide LOR and collapse area according to slope aspect

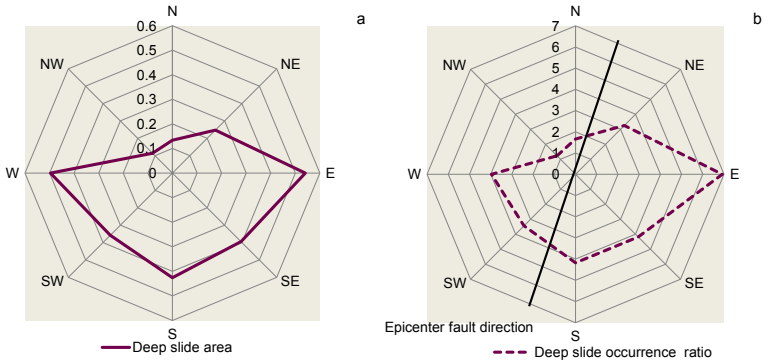

FIGURE 5.12: Deep slide LOR and collapse area according to slope aspect

direction of the failed slopes is almost perpendicular to the fault direction but is not the same as that for the other slide types. The relationship between the direction of the slope and the deep slide occurrence ratio is strong. The reason is probably that deep slides are strongly affected by the geological structure. However, to study the relationship between the slope facing direction and the fault direction in detail, comprehensive knowledge regarding the geological structure of the slopes is needed.

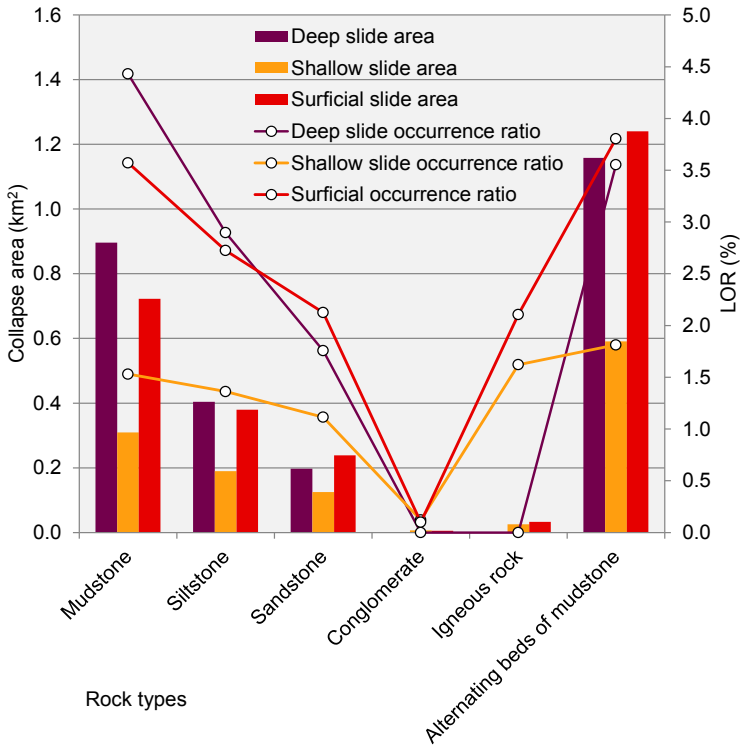

FIGURE 5.13: Occurrence ratio and collapse area according to rock type

5.4 Variation of Landslide Occurrence Ratio with Rock Type

Pre-existing landslide deposits are widespread and many landslides have occurred historically in and around the study area. The influence of rock type on the occurrence of landslides was analyzed considering and ignoring pre-existing landslide deposits. **Figure 5.13** shows the LOR of the three landslide types with respect to rock type. The three types of landslides exhibit similar trends. Especially, LORs are higher in mudstone and alternating beds of mudstone. **Figure 5.14** presents the recalculated LOR considering the pre-existing landslide deposits. The recalculation was done by taking into account the area occupied by old landslides as one of the rock features in the study area. The results in **Figure 5.14** exhibit almost the same LOR as those in **Figure 5.13**, but the deep slide occurrence ratio for pre-existing landslide topography is slightly different. The deep slide occurrence ratio increases when the pre-existing landslide deposits are considered. This finding indicates that deep slides are greatly influenced by the pre-existing landslide deposits. The sliding mechanism of a slope can be identified rationally

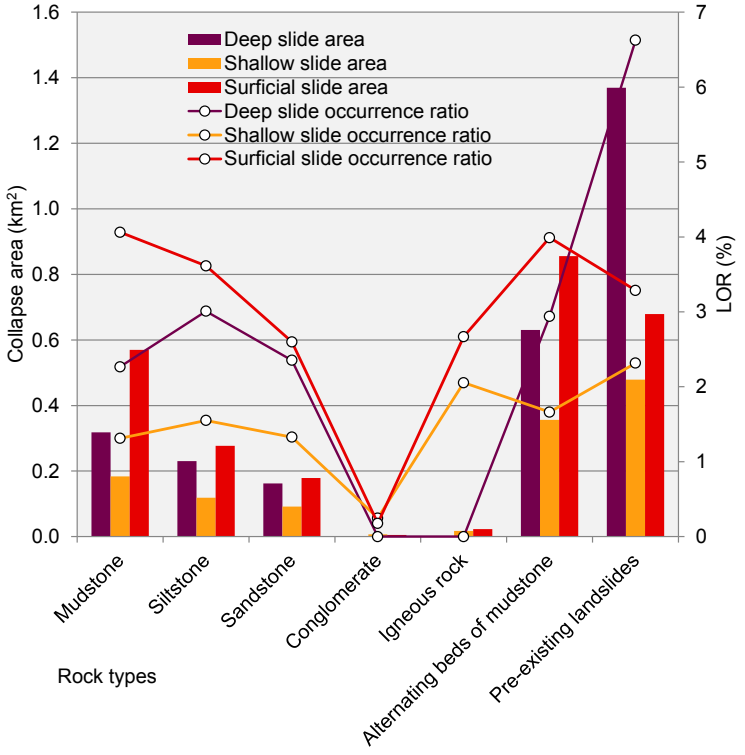

FIGURE 5.14: Occurrence ratio and collapse area according to rock type and pre-existing landslide deposits

by recognizing the shear strength of each rock type. However, it is difficult to characterize the sliding mechanism using existing data. For this reason a general description is used in this study.

Chapter 6

Identification of Shear Strength and Seismic Coefficient by Back Analyzing Surficial Slides

6.1 Overview of the Back Analysis

Earthquakes constitute one of the main triggering factors for instability of natural and man-made slopes. It is therefore essential to consider the seismic effects for designing slope stability, retaining walls, bridges and other engineering structures. Seismic stability of earth structures has been analyzed the early twentieth century. As result of such efforts, Terzhagi (1950) [15] formalized a method to analyze the seismic stability of slope by adding the earthquake force to the static-equilibrium analysis which later became known as pseudo-static analysis. Pseudo-static (PS) analysis is a widely accepted method for evaluating slope stability. In the PS procedure the effects of an earthquake are represented by constant horizontal and/or vertical accelerations. Stability is expressed in terms of a pseudo-static factor of safety calculated by limit equilibrium procedures. Limit equilibrium analyses consider force and/or moment equilibrium of a mass of soil above a potential failure surface. The first consideration of the pseudo-static approach to the analysis of seismic slope stability was done by by Terzaghi. The results of pseudo-static analyses are totally dependent on the value of the seismic coefficient. The seismic coefficient controls the pseudo-static force on the failure surface. Hence its

TABLE 6.1: Horizontal seismic coefficients from various studies

Investigator	Horizontal Seismic Coefficient, k_h
Terzhagi	0.1 (severe earthquakes) 0.2 (violent, destructive earthquakes) 0.5 (catastrophic earthquakes)
Seed	0.10 (M=6.50) 0.15 (M=8.25)
Marcuson	1/2 to 1/3 of PHA
Hynes-Griffin and Franklin	1/2 of PHA
California Division of Mines and Geology	0.15
JCOLD Japan	0.12-0.25
Crops of Engineering	0.1 (Major Earthquake) 0.15 (Great Earthquake)
PHA: Peak Horizontal Acceleration, in g's	

value is connected to some measures of the amplitude of the inertial force induced in the failure slope by the dynamic forces generated during the earthquake. The most difficult and important aspect of PS analysis is to is to select an appropriate pseudo-static coefficient (particularly k_h). **Table 6.1** shows the recommended values of horizontal seismic coefficient for design. Terzaghi proposed that the use of $k_h = 0.1$ for severe earthquakes (Rossi-Forel IX), $k_h = 0.2$ for violent and destructive earthquakes (Rossi-Forel = X), and $k_h = 0.5$ for catastrophic earthquakes. Seed (1979) [57] listed pseudo-static design criteria for dams and required a maximum factor of safety of 1.15 with pseudo-static coefficients of 0.10 to 0.15. The difference between each approach and resulting values is clearly evident in prior studies (**Table 6.1**). As shown in **Table 6.1** there are no specific rules when selecting a proper seismic coefficient for design. This study assumed that the horizontal seismic coefficient varied with from the epicenter fault line. It is important to determine the shear strength parameters on a failure surface for stability evaluation and engineering analysis of a landslide; these parameters are mainly determined by the test, back analysis method and engineering experience analogy method (Sonmez et al., 1998) [**?**]. Among these methods, the back calculation is a procedure which offers the opportunity to estimate the shear strength properties along the failure surface using the mathematical method. Soil strength calculation by back analysis avoids many of the problems related to laboratory testing, and is widely used, especially in association with landslide repair studies (Duncan and Stark, 1992) [19]. In this thesis back analysis is carried out to calculate the horizontal seismic coefficient according to the distance from the epicenter fault line and shear strength of the weathered soil.

6.2 Earthquake-Induced Surficial Slide

Variation of landslide occurrence ratio with distance from epicenter fault line can be seen in **Figure 6.1**. Surficial slide and shallow slide monotonically decreases when distance increases from the epicenter fault line. It reveals that the shaking motion decreases with the increase in distance from the epicenter fault line; on the contrary, the occurrence ratio of deep slide does not show a clear relationship between LOR and the distance from the epicenter fault line. Slope angle can be considered as one of the major causes of landslide susceptibility. In order to calculate mean slope angle of the landslide slope, 4m DEM data have been used. The relationship between landslides and slope gradient categories is shown in **Figure 6.2** . It shows surficial slide occurrence ratio increases with slope angle and this occurs because the shear stress in the slope generally increases with the slope angle. This result implies that slope angle is strongly correlated with surficial slides which induced by the earthquake. The shallow slide shows that the highest occurrence ratio at slope angles is between $25° - 35°$. Deep slide occurrence ratio increases with increasing slope gradient until a maximum is reached in the $25° - 30°$ category, and then generally decreases with increasing slope gradient. **Figure 6.3** shows the relationship between surficial slide occurrence ratio and slope angle values with distance from the epicenter fault line. LOR of lower slope angles are gently and higher slope angles steeply decrease with distance from the epicenter fault line. Assuming the seismic shaking decreases distance from the epicenter fault line due to attenuation of energy within the subsurface, back analysis is conducted to calculate seismic coefficient and shear strength of the weathered soil.

6.3 Probabilistic Approach to Calculate Failure Ratio

It is well known that the soil property is stochastically distributed. Many studies have suggested that the traditional deterministic methods of slope stability analyses should be replaced by the probabilistic method (McMahon, 1975; [43] Vanmarcke, 1980; [65] Priest and Brown, 1983; [49] Read and Lye, 1983 [53]). In the deterministic methods, the uncertainties in soil parameters are treated by setting the margin in the factor of safety. However, it is recognized that the factor of safety alone is not an adequate measurement for risk assessment in recent years. It is not clear how much safer a structure becomes

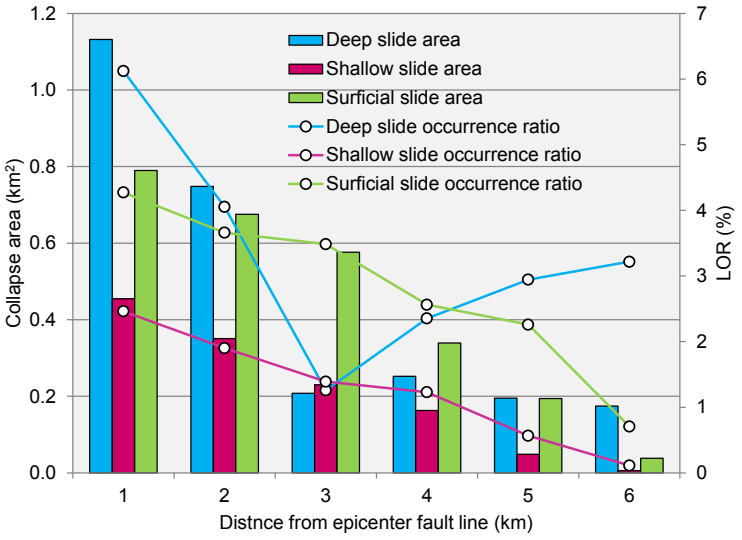

FIGURE 6.1: Landslide occurrence ratios with respect to distance from epicenter fault line in three types of slides

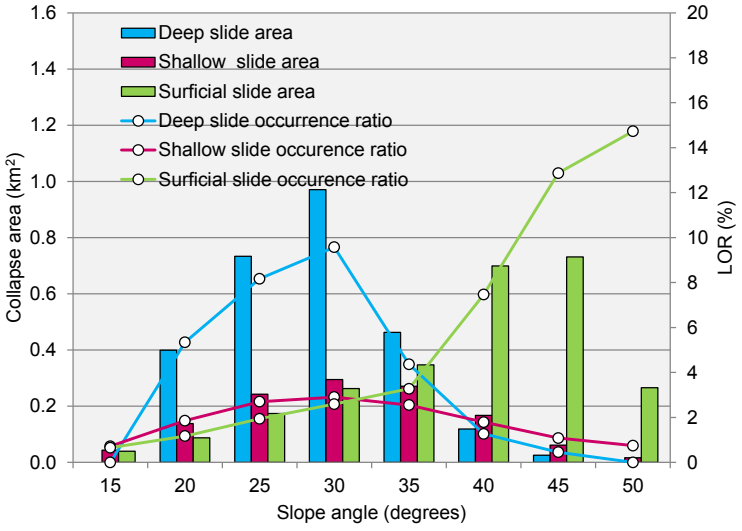

FIGURE 6.2: Landslide occurrence ratios with respect to slope angle for three types of slides

as the factor of safety increases (Duncan, 2000) [**?**]. The probability of failure of any structure can be generally expressed as (Melchers, 1987) [52]

$$P_f = p[R - S \leq 0] \tag{6.1}$$

where R and S express the resistance force and the sliding force at the slip line. **Figure 6.5** expresses the failure mechanism of surficial slides. The probability of failure for surficial slides is properly assessed by Equation 6.1. A limit state function $Z(X_i...X_n)$

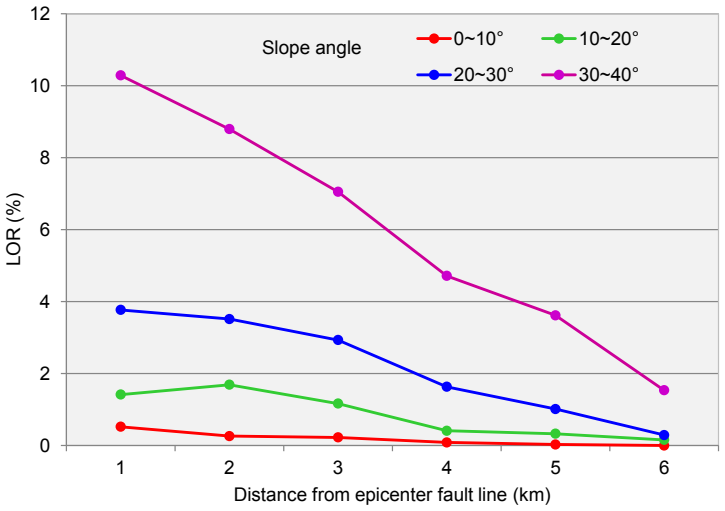

FIGURE 6.3: Slope angle and surficial slide occurrence ratio according to distance from epicenter fault line

is defined where $X_i ... X_n$ are basic variables, which separates the design space into failure and safe regions

$$Z(X_i ... X_n) > 0 \ (Safe \ region) \tag{6.2}$$

$$Z(X_i ... X_n) \leq 0 \ (Failure \ region) \tag{6.3}$$

The probability of the limit state can be expressed as

$$P_f = p[Z(R, S) \leq 0] \tag{6.4}$$

where Z is the 'limit state function'. It defines the limit state between the safe and the unsafe region. The limit state function for surficial slides is given by the following equation as the margin of safety 'Z' (Melchers, 1987) [52].

$$Z = R - S \tag{6.5}$$

The mean value and the standard deviation of Z are given as

$$\mu_Z = (\mu_R - \mu_S) \tag{6.6}$$

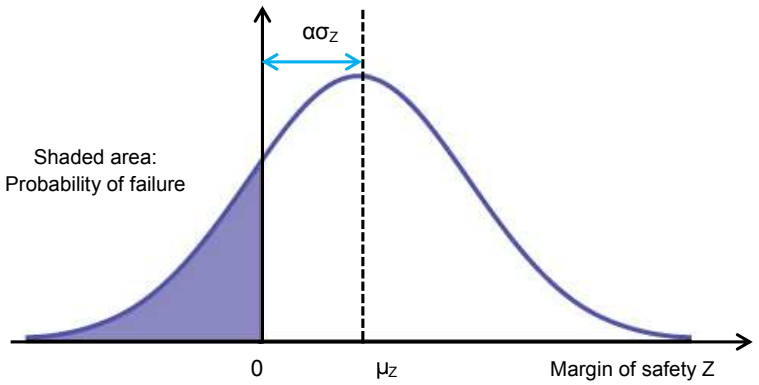

FIGURE 6.4: Normal distribution of safety margin Z, μ_Z is the mean, σ_Z is the standard deviation and α is the reliability index

$$\sigma_Z = \sqrt{(\sigma_R^2 + \sigma_S^2)} \tag{6.7}$$

where μ_R and μ_S are the means of R and S, respectively, and σ_R and σ_S are the standard deviations of R and S respectively. **Figure 6.4** shows the distribution of the safety margin (Z). If the (R) and (S) are normally distributed, the safety margin (Z) is also normally distributed (Melchers, 1987) [52]. The probability of failure can be expressed by integrating the shaded area in **Figure 6.5**. A random variable, which is normally distributed, is converted to a standard normal distribution by the following function.

$$H = \frac{Z - \mu_Z}{\sigma_Z} \tag{6.8}$$

The probability of failure P_f can be expressed in terms of a cumulative distribution function $\phi(H)$ for a standard normal random variable H. Then the probability of failure in **Figure 6.5** can be calculated as (Cornell, 1969) [12]:

$$P_f = \phi\Big(\frac{0 - \mu_Z}{\sigma_Z}\Big) = \phi\Big(-\frac{\mu_R - \mu_S}{\sqrt{(\sigma_R^2 + \sigma_S^2)}}\Big) = \phi(-\alpha) \tag{6.9}$$

where α is the reliability index.

$$P_f = \phi\Big(\frac{-(\mu_R - \mu_S)}{\sqrt{(\sigma_R^2 + \sigma_S^2)}}\Big) \times 100 \tag{6.10}$$

6.4 Seismic Stability of Surficial Slide

Evaluation of seismic slope stability is one of the most important factors in the design of earth structures. (**Figure 6.5**) shows the forces acting on a sliding block of soil above the sliding plane in the pseudo-static analysis. In this approach, the dynamic force is considered as the static force acting on the block above the sliding plane. Although the pseudo-static force generated by an earthquake originally has the vertical and horizontal components, the effect of vertical pseudo-static force on the sliding block is ignored as it has comparatively little effect on the slope stability (Hack et al., 2007) [27].

$$F_h = \left(\frac{Wa}{g}\right) = k_h W \tag{6.11}$$

Where, F_h - horizontal pseudo-static force acting on the sliding block

W - total weight of sliding block

a - horizontal acceleration at ground surface due to earthquake

g - acceleration of gravity

k_h- seismic coefficient

It is assumed that the sliced element of width b and depth h on the imaginary sliding plane have an inclination of β and parallel to the soil surface. The forces Q_L, Q_R acting on the vertical sides of the element are assumed to exactly balance each other (Leynaud et al., 2004) [42].

The slope is considered infinite, inter slice forces are parallel to the slope and cancel each other out ($Q_L = Q_R$) so one gets:

$$S = \gamma_t.h(sin\beta.cos\beta + k_h.cos^2\beta) \tag{6.12}$$

where, γ_t is the unit weight of the soil

$$Z = R - \gamma_t.h(sin\beta.cos\beta + k_h cos^2\beta) \tag{6.13}$$

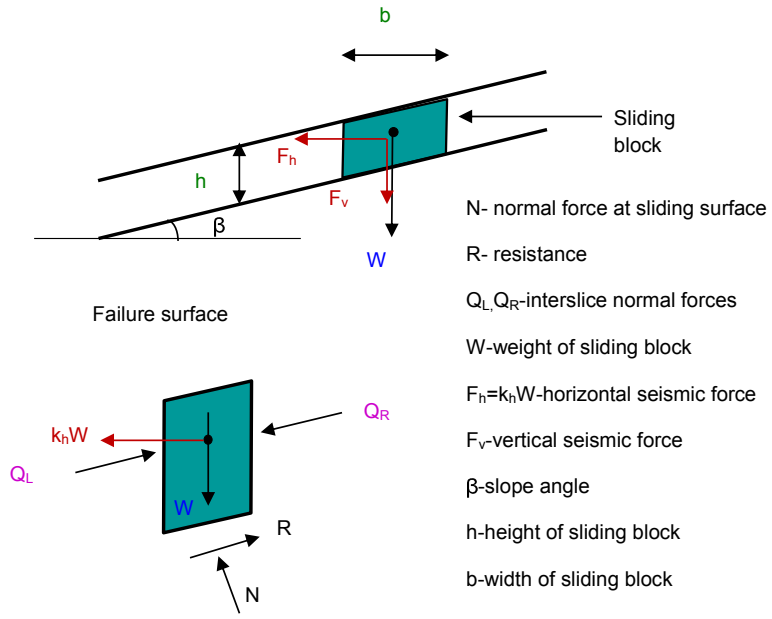

FIGURE 6.5: Force digram of sliding block in the context of surficial slide

6.5 Back Analysis of Uncertainties

This thesis examines the seismic coefficient during the 2004 Mid-Niigata prefecture earthquake and estimates the shear strength of the weathered soil logically. Coefficient of variation (COV) is a useful measurement for comparison of relative deviation between individual data sets with different means. However, the COV values of soil parameters are difficult to decide with confidence due to the lack of prominent data and inherent spatial variability. Therefore estimated COV values of soil parameters can vary within a wide range. Many researchers have made significant efforts to estimate COVs of soil properties. Kulhawy et al. (1991) [26] estimated the coefficients of variation for soil index properties (liquid limit, plastic limit, unit weight, initial void ratio) and soil performance properties (effective friction angle, undrained shear strength, and compression index) through an extensive literature review. It was estimated that the COV of unit weight for all soil types varied between 2%-12%. In contrast, the stochastic properties of sliding depth and seismic coefficient are very much unknown. Although the sliding depth of surficial slide is defined as being less than 1m, apparent that it is distributed widely. The seismic coefficient working to slope is generally varied due to slope direction and vibration property of the slope even though the distance from the epicenter fault line is the same. By assuming these variables are random variables of normal distribution, the back analysis can be easily implemented. However, they are expressed using several

TABLE 6.2: Statistics of uncertain parameters

Parameter	Mean	COV
$h(m)$	0.8	0.2
	0.9	0.2
	1.0	0.2
k_h		0.22
		0.32
		0.42
$\gamma_t(kN/m^3)$	17.5	0.1 (Kulhawy et al., (1991)) [26]

models as shown in **Table 6.2** as case studies. Let μ_R, μ_{γ_t}, μ_h, and μ_{kh} denote the average resistance force, average unit weight, average sliding depth, and average seismic coefficient at the sliding plane, respectively. With the above discussion, the statistics of uncertain parameters can be shown in **Table 6.2**. Mean and standard deviation of sliding force can be calculated using Equations 6.14 and 6.15 (Macias and Oliveira, 2012)) [58].

$$\mu_S = \mu_{\gamma_t}\mu_h(sin\beta.cos\beta + \mu_{k_h}cos^2\beta) \tag{6.14}$$

$$\begin{aligned}\sigma_S^2 = \; & sin^2\beta.cos^2\beta(\sigma^2_{\gamma_t}.\sigma^2_h + \mu^2_{\gamma_t}.\sigma^2_h + \mu^2_h.\sigma^2_{\gamma_t}) + cos^4\beta(\sigma^2_{kh}.\sigma^2_{\gamma_t}.\sigma^2_h + \\ & \sigma^2_{kh}.\sigma^2_{\gamma_t}.\mu^2_h + \sigma^2_{kh}.\mu^2_{\gamma_t}.\sigma^2_h + \sigma^2_{Kh}.\mu^2_{\gamma_t}.\mu^2_h + \mu^2_{kh}.\sigma^2_{\gamma_t}.\sigma^2_h + \\ & \mu^2_{kh}.\sigma^2_{\gamma_t}.\mu^2_h + \mu^2_{kh}.\mu^2_{\gamma_t}.\sigma^2_h)\end{aligned} \tag{6.15}$$

In the back analysis, it is furthermore assumed that the probability of failure (calculated from Equation 6.11) equates to the surficial slide occurrence ratio which is obtained from from GIS-based analysis. In this approach, the best estimation of system parameters is obtained by minimizing the residual sum of squares (which is defined as the difference between observed LOR of surficial slide and the calculated LOR by the back calculated uncertain parameters).

6.6 Results of Back Analysis

Figure 6.6 to 6.8 show the back analyzed seismic coefficient curves for distance from the epicenter fault line. The seismic coefficient is found to decrease with distance from the epicenter fault line. Back analyzed shear strength values are indicated in **Table 6.3**.

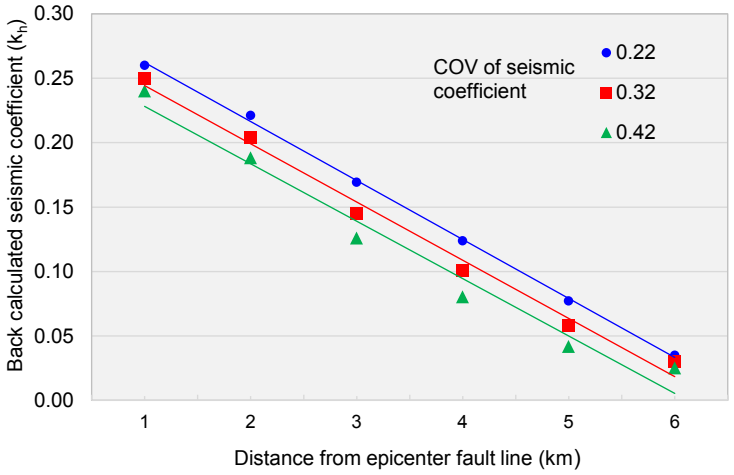

FIGURE 6.6: Back calculated seismic coefficient when ($\mu_h = 0.8m$)

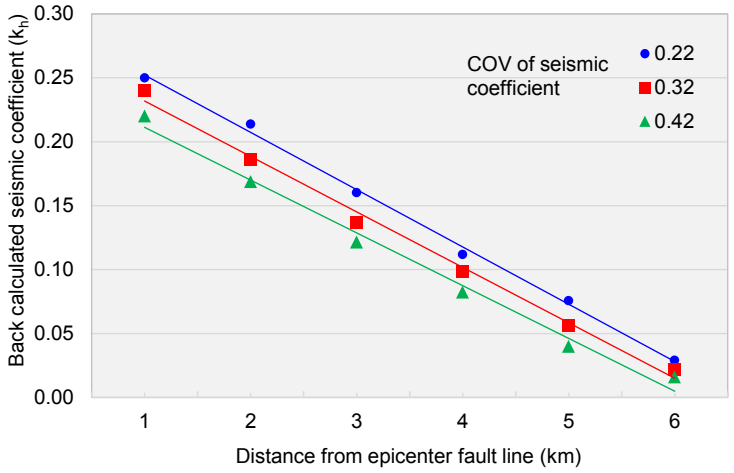

FIGURE 6.7: Back calculated seismic coefficient when ($\mu_h = 0.9m$)

TABLE 6.3: Back calculated uncertain parameters

$h(m)$	COV of (k_h)	k_h d=1	2	3	4	5	6	L
0.8	0.22	0.260	0.221	0.169	0.124	0.077	0.035	14.63
	0.32	0.250	0.204	0.145	0.101	0.058	0.030	14.81
	0.42	0.240	0.188	0.126	0.080	0.042	0.025	15.06
0.9	0.22	0.250	0.214	0.160	0.112	0.076	0.029	16.46
	0.32	0.240	0.186	0.137	0.099	0.056	0.022	16.67
	0.42	0.220	0.169	0.121	0.082	0.040	0.016	16.94
1.0	0.22	0.240	0.198	0.154	0.110	0.070	0.025	17.76
	0.32	0.230	0.177	0.134	0.090	0.054	0.018	17.96
	0.42	0.220	0.160	0.110	0.080	0.037	0.010	18.22

d:Distance from epicenter fault line (km)
L:Shear strength of the weathered soil (kPa)

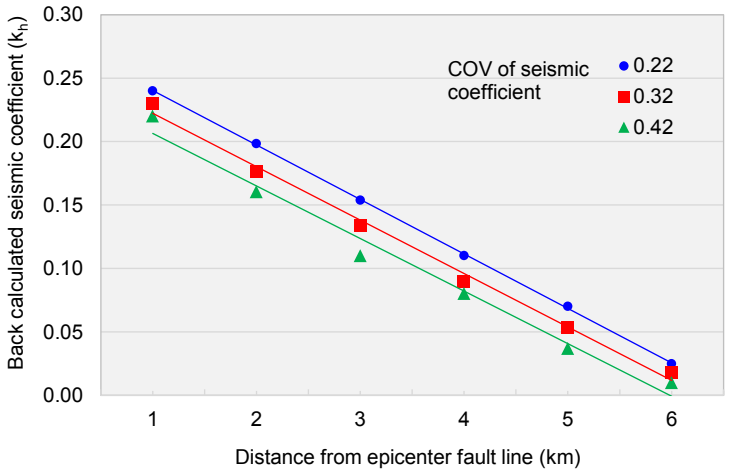

FIGURE 6.8: Back calculated seismic coefficient when ($\mu_h = 1.0m$)

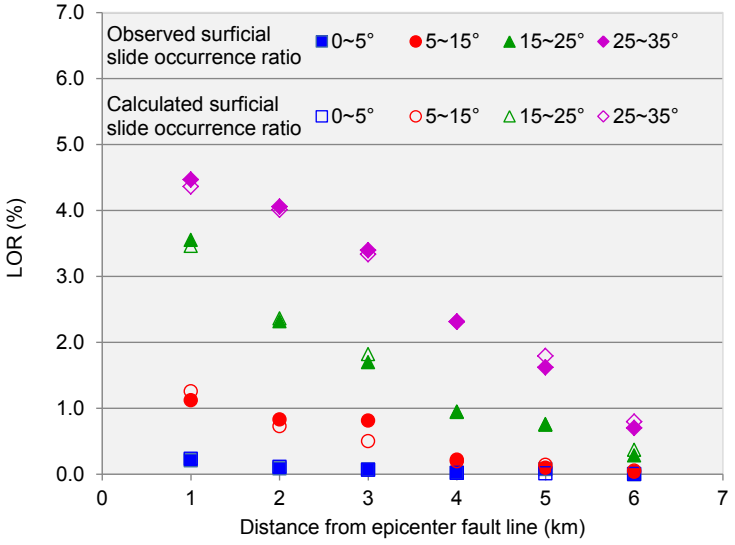

FIGURE 6.9: Comparison of the observed surficial slide occurrence ratio with calculated surficial slide occurrence ratio

Coefficient of variation for seismic coefficient varies between 0.22 to 0.42. The coefficient of variation for the seismic coefficient is set at a wider range because the seismic coefficient applying to the slope widely varies due to slope direction. In this study, In this study, the impact of greater variance in seismic coefficient is surveyed to examine the physical validity of results obtained by using the back analysis method. It can be seen that the seismic coefficient decreases when the coefficient of variation increases. Referring to the effect of sliding depth, the seismic coefficient is obtain as being slightly higher with the shallower sliding depth. Nevertheless it is found to be almost the same as that of sliding depth. The largest seismic coefficient ranged from 0.22 to 0.26 at 1km

from the epicenter fault line. Conversely, the average shear strength is comparatively affected by sliding depth. It becomes greater with the deeper sliding depth. The average shear strength of weathered soil at slope surface is analyzed as around 14.63kPa and 18.22kPa for sliding depth of h=0.8m and h=1m. The verification of the back analysis is done by comparing the analyzed failure ratio and the observed surficial slide occurrence ratio. The results in **Figure 6.9** show that the analyzed surficial slide occurrence ratio (failure ratio calculated from the probability approach) using back calculated seismic coefficient and shear strength coincide well with the observed results, indicating that this method is indeed effective.

Chapter 7

Conclusion and Future Work

7.1 Summary of the Research

The 2004 Mid-Niigata Prefecture earthquake caused extensive damage due to landslides throughout the Yamakoshi area of Japan. The landslide types studied were surficial, shallow, and deep slides. The majority of the landslides were surficial slide which thickness less than 1m. Even though the number of deep slides was relatively small, they contributed significantly to the total collapse area. Hence we defined a new index as LOR to find the correlation between landslide distribution with each geologic and geomorphic factor. The LOR is defined as the ratio of the collapse area to the total area, where the collapse area is the surface area of landslide scars for a given class of a given predisposing factor, while the total area is the total surface area for a given class of a given predisposing factor. These predisposing factors include the distance from the epicenter fault line, slope angle, distance from rivers and ponds, and rock type, slope structure, and slope aspect. Two topographic parameters, the slope angle and slope aspect, were correlated with the LOR. The slope angle and aspect were calculated from a 10 m $\times$ 10 m DEM. The study area consists of many paddy fields and fish ponds, but the particular regional features of the area increase the risk of the slope failure due to penetration of surface water into the soils and rocks. By assuming that the high ground water level exists near water sources such as rivers and ponds, we investigate the effect of ground water level for occurrences of the landslide. In order to assess bedding plane orientation for occurrences of landslide distribution this research presented a method to determine geometric alignment between topography and the orientation of geological

bedding planes. Since the strike and dip directions are angular values, the polarity of the bedding plane had to account for the prediction of bedding measurements. Inverse Distance Weighted (IDW) is used to interpolate spatial fields of dip direction and dip from point measurements of strike and dip. Major slope types were identified (dip slope, reverse dip slope, and horizontal dip slope) by correlating estimated dip angle and dip direction together with slope angle and slope aspect which is derived from the DEM. The proposed method provides an efficient means for estimating the topographic/bedding plane relationship over large areas in macroscopic view. These hilly areas have suffered many earthquakes throughout history. Hence Pre-existing landslide deposits are very common in and around this area. Therefore this study assesses the pre-existing landslide influence for earthquake-induced landslide distribution. Surficial slide induced by the earthquake reveals unique behaviour with slope angle and distance from epicenter fault line. These results helped to calculate the shear strength of weathered soil and horizontal seismic coefficient through back analysis procedure. Furthermore this study conducted the back analysis to estimate the shear strength of the weathered soil and seismic coefficient.

7.2 Results and Discussion

This thesis discussed three different types of earthquake-induced landslides n the 2004 Mid-Niigata prefecture and their causes. The surficial slide occurrence ratio generally increases with the slope angle, but deep slides and shallow slides do not show a continuous increase. Shallow slopes between 25° and 35° are more susceptible to landsliding. The deep slide occurrence ratio increases with increasing slope gradient until a maximum is reached in the 25°–30° range and then generally decreases with increasing slope gradient. The slope angle is an important factor in determining the stability of the slope, but there are other factors. Surficial and shallow slopes that face parallel to the fault direction are more prone to failure. However, the trend is moderate and the change in the LOR with respect to the direction of the slope is continuous. The deep slide occurrence ratio is higher for slopes that face perpendicular to the fault direction. Because the obtained relationship is strong, it can be concluded that deep slides are strongly affected by the geological structure. As historical landslides significantly modify the subsurface geology and topography, the classification of rock types is not applicable for evaluating

the properties of the ground. In this study, analysis considering and ignoring pre-existing landslide deposits is conducted to investigate the effect of pre-existing landslide deposits on the LOR. It is found that most of the deep slides are concentrated in the pre-existing landslide deposits. The morphostructural influence on landslide occurrence is investigated from a macroscopic perspective. The shallow slide and surficial slide occurrence ratios are more or less equal for all the slope types. This finding indicates that shallow and surficial slides occur independently of the macroscopic structure of the slope. Deep slides occur preferentially on dip slopes, but the occurrence ratio of pre-existing landslide deposits is also higher. It can be seen that deep slides are influenced mainly by the bedding plane (parallel bedding slopes are more susceptible to collapse) and pre-existing landslide deposits.

However, surficial slides are correlated well with slope angle and distance from the epicenter fault line. Hence stochastic analysis was carried out to survey the shear strength of the weathered soil and seismic coefficient. The homogeneity of weathered soil is assumed to calculate the weathered soil's shear strength. Back analysis is based on the pseudo-static analysis for the surficial sliding model. The variance of parameters in the model is taken into account when using the stochastic approach. This analysis is implemented to express the landslide occurrence ratio for various angles of slopes and distances from the epicenter fault line. The back analysis results are discussed by assuming three different coefficients of variation for seismic intensity coefficient. According to the obtained results of the back analysis, the seismic coefficient was 0.26 - 0.22 near the epicentral area and 0.035-0.010 at the 6km from the epicenter fault line. Shear strength of the weathered soil varied between $14.63 - 18.22kPa$. The seismic coefficient is found to be similar to previous research studies. However, the accuracy and resolution in the seismic coefficient is higher due to GIS-based analysis and the detailed information in 4504 records of surficial slides. The effects of uncertainties such as sliding depth and its variance are surveyed by parametric study and the shear strength of weathered soil at slope surface is estimated. It is generally surveyed by field tests. However, the obtained data is point wise and it is difficult to grasp the macroscopic property of the ground. By regarding the surificial slides induced by the past earthquake as the in-situ real scale shaking table test, the shear strength is logically estimated.

7.3 Limitations and Future Work

As a result of the catastrophic earthquake that hit Japan's Mid-Niigata prefecture in 2004, a huge landslide occurred. In addition to that shook the whole environmental surrounding the area, this worsened the risk of slope failure during the rainy season. Since then, researchers have encountered many challenges for mitigating not only earthquake-induced disasters but also the subsequent disasters after the earthquake. Prior to the Mid-Niigata Prefecture earthquake typhoon 23, went through the Chuetsu area and resulted in more than 100mm of rainfall being recorded. Some researchers (Onoue et al., 2006 [45] and Deng et al., 2011 [17]) assumed that the landslides were triggered by the increase in pore water pressure inseam layers. In addition to that rising ground water table, decreasing suction, seepage erosion, subsequent infiltration may also lead to slope failure. However, these are issues need to be addressed in future studies.

Appendix A

Publications

Publications

- Surangani Bandara and Satoru Ohtsuka:Spatial distribution of landslides induced by the 2004 Mid-Niigata prefecture earthquake, Japan, *Landslides*, DOI 10.1007/s10346-017-0819-6, 2017
- Surangani Bandara, Satoru Ohtsuka, Tsukasa Iwabe, Yasuyuki Miyaki, Koichi Isobe: Analysis of geological and geomorphological characteristics of landslides triggered by 2004 Chuethsu earthquake in Japan, INTERPRAEVENT 2014 in the Pacific Rim, 2014
- KMS Bandara and Satoru Ohtsuka: The 14th International Conference of the International Association for Computer Methods and Advances in Geomechanics (14IACMAG), pp1903–1906, 2014
- Surangani Bandara and Satoru Ohtsuka:The 3rd International GIGAKU conference in Nagaoka (IGCN2014), Seismic landslide hazard assessment and evaluation of factors controlling landslides in 2004 Chuetsu earthquake, pp.90, 2014
- Surangani Bandara and Satoru Ohtsuka: Characteristics of Surficial Slides and Deep Slides Induced by 2004 Mid-Niigata Prefecture Earthquake, Sustainable Technology and Practice for Infrastructure and Community Resilience (IGNITE-AICCE'17), 2017 (submitted)

Bibliography

[1] Japan Meteorological Agency. (press release materials 28th report on november 10). *http://www.seisvol.kishou.go.jp/eq/gaikyo/kaisetsu200411100600.pdf*, 2004.

[2] Pietro Aleotti and Robin Chowdhury. Landslide hazard assessment: summary review and new perspectives. *Bulletin of engineering geology and the Environment*, 58(1):21–44, 1999.

[3] Surangani Bandara and Satoru Ohtsuka. Spatial distribution of landslides induced by the 2004 Mid-Niigata prefecture earthquake, Japan. *Landslides*, pages 1–10, 2017.

[4] Muhammad Basharat, Joachim Rohn, Mirza Shahid Baig, and Muhammad Rustam Khan. Spatial distribution analysis of mass movements triggered by the 2005 Kashmir earthquake in the northeast Himalayas of Pakistan. *Geomorphology*, 206:203–214, 2014.

[5] A Carrara, M Cardinali, R Detti, F Guzzetti, V Pasqui, and P Reichenbach. GIS techniques and statistical models in evaluating landslide hazard. *Earth Surface Processes and Landforms*, 16(5):427–445, 1991.

[6] Alberto Carrara. Multivariate models for landslide hazard evaluation. *Mathematical Geology*, 15(3):403–426, 1983.

[7] Kang-tsung Chang and Bor-wen Tsai. The effect of DEM resolution on slope and aspect mapping. *Cartography and Geographic Information Systems*, 18(1):69–77, 1991.

[8] Masahiro Chigira, Wen-Neng Wang, Takahiko Furuya, and Toshitaka Kamai. Geological causes and geomorphological precursors of the tsaoling landslide triggered by the 1999 chi-chi earthquake, taiwan. *Engineering Geology*, 68(3):259–273, 2003.

[9] Masahiro Chigira and Hiroshi Yagi. Geological and geomorphological characteristics of landslides triggered by the 2004 Mid Niigta prefecture earthquake in Japan. *Engineering Geology*, 82(4):202–221, 2006.

[10] T Edwin Chow and Michael E Hodgson. Effects of lidar post-spacing and DEM resolution to mean slope estimation. *International Journal of Geographical Information Science*, 23(10):1277–1295, 2009.

[11] L Claessens, GBM Heuvelink, JM Schoorl, and A Veldkamp. DEM resolution effects on shallow landslide hazard and soil redistribution modelling. *Earth Surface Processes and Landforms*, 30(4):461–477, 2005.

[12] C Allin Cornell. A probability-based structural code. *Journal Proceedings*, 66(12):974–985, 1969.

[13] DM Cruden. Limits to common toppling. *Canadian Geotechnical Journal*, 26(4):737–742, 1989.

[14] FC Dai, CF Lee, JXuZW Li, and ZW Xu. Assessment of landslide susceptibility on the natural terrain of Lantau Island, Hong Kong. *Environmental Geology*, 40(3):381–391, 2001.

[15] FC Dai, C Xu, X Yao, L Xu, XB Tu, and QM Gong. Spatial distribution of landslides triggered by the 2008 ms 8.0 Wenchuan earthquake, China. *Journal of Asian Earth Sciences*, 40(4):883–895, 2011.

[16] Marcello De Michele, Daniel Raucoules, Julia De Sigoyer, Manuel Pubellier, and Nicolas Chamot-Rooke. Three-dimensional surface displacement of the 2008 May 12 Sichuan earthquake (China) derived from synthetic aperture radar: evidence for rupture on a blind thrust. *Geophysical Journal International*, 183(3):1097–1103, 2010.

[17] Jianliang Deng, Hiroshi Kameya, Yukika Miyashita, Jiro Kuwano, Reiko Kuwano, and Junichi Koseki. Study on dip slope failure at Higashi Takezawa induced by 2004 Niigata-ken Chuetsu earthquake. *Soils and foundations*, 51(5):929–943, 2011.

[18] Yongxin Deng, John P Wilson, and BO Bauer. Dem resolution dependencies of terrain attributes across a landscape. *International Journal of Geographical Information Science*, 21(2):187–213, 2007.

[19] J Michael Duncan. Factors of safety and reliability in geotechnical engineering. *Journal of Geotechnical and Geoenvironmental Engineering*, 126(4):307–316, 2000.

[20] J Michael Duncan and Timothy D Stark. Soil strengths from back analysis of slope failures. In *Stability and Performance of Slopes and Embankments II:*, pages 890–904. ASCE, 1993.

[21] ESRI, P. A Burrough, and R.A McDonell. Principles of Geographical Information Systems. *Oxford University Press, New York*, page 190, 1998.

[22] Peter G Fookes and D Dene Wilson. The geometry of discontinuities and slope failures in siwalik clay. *Geotechnique*, 16(4):305–320, 1966.

[23] RA Freeze and JA Cherry. Groundwater. *Prentice-Hall International. New Jersey: Englewood Cliffs*, 1979.

[24] Niigata Prefectural Government. Niigata prefecture report on damage in the 2004 Niigata-Chuetsu earthquake. *No. 174, final report)*, 2009.

[25] G Grelle, P Revellino, A Donnarumma, and FM Guadagno. Bedding control on landslides: a methodological approach for computer-aided mapping analysis. *Natural Hazards and Earth System Sciences*, 11(5):1395, 2011.

[26] Kulhawy H, Roth NJS, and Grigoriu NB. Some statistical evaluations of geotechnical properties. *VI ICASP*, pages 705–712, 1991.

[27] Robert Hack, Dinand Alkema, Gerard AM Kruse, Noud Leenders, and Lucia Luzi. Influence of earthquakes on the stability of slopes. *Engineering Geology*, 91(1):4–15, 2007.

[28] Edwin L Harp and Randall W Jibson. Landslides triggered by the 1994 Northridge, California, earthquake. *Bulletin of the Seismological Society of America*, 86(1B):S319–S332, 1996.

[29] JN Hutchinson. Mass movementmass movement. In *Geomorphology*, pages 688–696. Springer, 1968.

[30] JN Hutchinson. General report: morphological and geotechnical parameters of landslides in relation to geology and hydrogeology: Proc 5th international symposium on landslides, Lausanne, 10–15 July 1988v1, p3–35. publ Rotterdam: AA

Balkema, 1988. In *International Journal of Rock Mechanics and Mining Sciences & Geomechanics Abstracts*, volume 26, page 88. Pergamon, 1989.

[31] Geographical Survey Institute. (2004a) Press release materials on 29 Oct. *http://www.gsi.go.jp/WNEW/PRESS-RELEASE/2004/1029-3.htm (in Japanese)*, 2004.

[32] Yujing Jiang, Chunxiang Wang, and Xiaodong Zhao. Damage assessment of tunnels caused by the 2004 Mid Niigata prefecture earthquake using Hayashi's quantification theory type II. *Natural hazards*, 53(3):425–441, 2010.

[33] KA Johnson and N Sitar. Hydrologic conditions leading to debris-flow initiation. *Canadian Geotechnical Journal*, 27(6):789–801, 1990.

[34] David K Keefer. Landslides caused by earthquakes. *Geological Society of America Bulletin*, 95(4):406–421, 1984.

[35] David K Keefer. Statistical analysis of an earthquake-induced landslide distribution—the 1989 Loma Prieta, california event. *Engineering Geology*, 58(3):231–249, 2000.

[36] Bijan Khazai and Nicholas Sitar. Evaluation of factors controlling earthquake-induced landslides caused by Chi-Chi earthquake and comparison with the Northridge and Loma Prieta events. *Engineering geology*, 71(1):79–95, 2004.

[37] D Scott Kieffer, Randy Jibson, Ellen M Rathje, and Keith Kelson. Landslides triggered by the 2004 Niigata ken Chuetsu, Japan, earthquake. *Earthquake Spectra*, 22(S1):47–73, 2006.

[38] I Kobayashi, M Tateishi, T Yoshioka, and M Shimazu. Geology of the Nagaoka district. *Geological Survey of Japan, Quadrangle Series (Scale 1 : 50,000)*, 1991.

[39] K Koketsu, K Hikima, H Miyake, and Y Tanaka. The Mid Niigata prefecture earthquake in 2004–strong motion and source process. *http://taro.eri.u-tokyo.ac.jp/saigai/chuetsu/chuetsu.html*, 2004.

[40] Saro Lee, Jawon Choi, and Ik Woo. The effect of spatial resolution on the accuracy of landslide susceptibility mapping: a case study in Boun, Korea. *Geosciences Journal*, 8(1):51–60, 2004.

[41] S Leroueil, J Vaunat, L Picarelli, J Locat, H Lee, and RM Faure. Geotechnical characterisation of slope movements. In *7th International Symposium on Landslides*, volume 1, pages 53–74. AA Balkema, 1996.

[42] Didier Leynaud, Jürgen Mienert, and Farhad Nadim. Slope stability assessment of the Helland Hansen area offshore the Mid-Norwegian margin. *Marine Geology*, 213(1):457–480, 2004.

[43] BK McMahon et al. Probability of failure and expected volume of failure in high rock slopes. In *Second Australia-New Zealand Conference on Geomechanics*, page 308. Institution of Engineers, Australia, 1975.

[44] F Noverraz, C Bonnard, H Dupraz, and L Huguenin. Grands glissements de versants et climat. rapport final pnr 31. Technical report, VDF, 1998.

[45] Atsuo Onoue, Akihiko Wakai, Keizo Ugai, Kunihiro Higuchi, Kiyoshi Fukutake, Hiroyuki Hotta, Seiichiro Kuroda, and Hideaki Nagai. Slope failures at Yokowatashi and Nagaoka College of Technology due to the 2004 Niigata-ken Chuetsu earthquake and their analytical considerations. *Soils and Foundations*, 46(6):751–764, 2006.

[46] N Oyagi, S Uchiyama, and T Inokuchi. Map of landslides caused by the 2004 Niigata-ken Chuetsu (Mid Niigata) earthquake (mjma= 6.8). *Technical Note of the National Research Institute for Earth Science and Disaster Prevention*, 317:1–37, 2008.

[47] George Papathanassiou, Sotiris Valkaniotis, Athanassios Ganas, and Spyros Pavlides. GIS-based statistical analysis of the spatial distribution of earthquake-induced landslides in the island of Lefkada, Ionian Islands, Greece. *Landslides*, 10(6):771–783, 2013.

[48] Mario Parise and Randall W Jibson. A seismic landslide susceptibility rating of geologic units based on analysis of characteristics of landslides triggered by the 17 January, 1994 Northridge, California earthquake. *Engineering geology*, 58(3):251–270, 2000.

[49] SD Priest and ET Brown. Probabilistic stability analysis of variable rock slopes. *Institution of Mining and Metallurgy Transactions*, 92, 1983.

[50] Shengwen Qi, Qiang Xu, Hengxing Lan, Bing Zhang, and Jianyou Liu. Spatial distribution analysis of landslides triggered by 2008.5. 12 Wenchuan earthquake, China. *Engineering Geology*, 116(1):95–108, 2010.

[51] Wang Qi, Qiao Xuejun, Lan Qigui, Jeffrey Freymueller, Yang Shaomin, Xu Caijun, Yang Yonglin, You Xinzhao, Tan Kai, and Chen Gang. Rupture of deep faults in the 2008 Wenchuan earthquake and uplift of the Longmen Shan. *Nature Geoscience*, 4(9):634–640, 2011.

[52] Melchers RE. Structural reliability. In *Analysis and Prediction*, page 400. Wiley, 1987.

[53] JRL Read, GN Lye, et al. Pit slope design methods: Bougainville copper limited open cut. In *5th ISRM Congress*. International Society for Rock Mechanics, 1983.

[54] B Sander. An introduction to the study of the fabric of the geological bodies. *Oxford. Pergamon*, 1970.

[55] Hiroshi P Sato, Tatsuo Sekiguchi, Ryoichi Kojiroi, Yoshinori Suzuki, and Makoto Iida. Overlaying landslides distribution on the earthquake source, geological and topographical data: the Mid Niigata prefecture earthquake in 2004, Japan. *Landslides*, 2(2):143–152, 2005.

[56] HP Sato and EL Harp. Interpretation of earthquake-induced landslides triggered by the 12 May 2008, m7.9 Wenchuan earthquake in the Beichuan area, Sichuan Province, China using satellite imagery and Google Earth. *Landslides*, 6(2):153–159, 2009.

[57] H Bolton Seed. Considerations in the earthquake-resistant design of earth and rockfill dams. *Geotechnique*, 29(3):215–263, 1979.

[58] Antonio Seijas-Macías and Amílcar Oliveira. An approach to distribution of the product of two normal variables. *Discussiones Mathematicae Probability and Statistics*, 32(1-2):87–99, 2012.

[59] MJ Selby. Hillslope materials and processes. *Oxford: Oxford University Press*, 1993.

[60] Zheng-Kang Shen, Jianbao Sun, Peizhen Zhang, Yongge Wan, Min Wang, Roland Bürgmann, Yuehua Zeng, Weijun Gan, Hua Liao, and Qingliang Wang. Slip maxima

at fault junctions and rupturing of barriers during the 2008 Wenchuan earthquake. *Nature Geoscience*, 2(10):718–724, 2009.

[61] K Shiono. Introduction to geometric vector for geologic mapping: Numerical analyses of orientation data. *Geoinformatics*, 19(1):37, 2008.

[62] RC Sidle and H Ochiai. Landslides: processes, prediction, and land use. American Geophysical Union, Washington, p 312. Technical report, 2006.

[63] H Sonmez, R Ulusay, and C Gokceoglu. A practical procedure for the back analysis of slope failures in closely jointed rock masses. *International Journal of Rock Mechanics and Mining Sciences*, 35(2):219–233, 1998.

[64] Theodore WJ van Asch, Jean-Philippe Malet, Ludovicus PH van Beek, and David Amitrano. Techniques, issues and advances in numerical modelling of landslide hazard. *Bulletin de la Société géologique de France*, 178(2):65–88, 2007.

[65] EH Vanmarcke. Probabilistic stability analysis of earth slopes. *Engineering Geology*, 16(1-2):29–50, 1980.

[66] David J Varnes. Landslide types and processes. *Special report*, 28:20–47, 1954.

[67] David J Varnes. Slope movement types and processes. *Special report*, 176:11–33, 1978.

[68] HB Wang, Kyoji Sassa, and WY Xu. Analysis of a spatial distribution of landslides triggered by the 2004 Chuetsu earthquakes of Niigata prefecture, Japan. *Natural Hazards*, 41(1):43, 2007.

[69] Wen-Neng Wang, Masahiro Chigira, and Takahiko Furuya. Geological and geomorphological precursors of the chiu-fen-erh-shan landslide triggered by the Chi-chi earthquake in central Taiwan. *Engineering Geology*, 69(1):1–13, 2003.

[70] Wen-Neng Wang, Huei-Long Wu, Hiroyuki Nakamura, Shang-Chih Wu, Shoung Ouyang, and Ming-Fang Yu. Mass movements caused by recent tectonic activity: the 1999 Chi-chi earthquake in central Taiwan. *Island Arc*, 12(4):325–334, 2003.

[71] Wang Wen-Neng, Hiroyuki Nakamura, Satoshi Tsuchiya, and Chen Chih-Ching. Distributions of landslides triggered by the Chi-Chi earthquake in central Taiwan on September 21, 1999. *Landslides*, 38(4):318–326, 2002.

[72] Chen Xiaoli, Zhou Qing, and Liu Chunguo. Distribution pattern of coseismic landslides triggered by the 2014 Ludian, Yunnan, China Mw6. 1 earthquake: special controlling conditions of local topography. *Landslides*, 12(6):1159–1168, 2015.

[73] Chong Xu, Xiwei Xu, Xin Yao, and Fuchu Dai. Three (nearly) complete inventories of landslides triggered by the May 12, 2008 Wenchuan Mw 7.9 earthquake of China and their spatial distribution statistical analysis. *Landslides*, 11(3):441–461, 2014.

[74] Xiwei Xu, Xueze Wen, Guihua Yu, Guihua Chen, Yann Klinger, Judith Hubbard, and John Shaw. Coseismic reverse-and oblique-slip surface faulting generated by the 2008 Mw 7.9 Wenchuan earthquake, China. *Geology*, 37(6):515–518, 2009.

[75] Xiwei XU, Guihua YU, Guihua Chen, Yongkang Ran, Chenxia LI, Yuegau Chen, and Chungpai Chang. Parameters of coseismic reverse-and oblique-slip surface ruptures of the 2008 Wenchuan earthquake, eastern Tibetan Plateau. *Acta Geologica Sinica (English edition)*, 83(4):673–684, 2009.

[76] Zhiqin Xu, Shaocheng Ji, Haibing Li, and Liwei Hou. Uplift of the longmen shan range and the wenchuan earthquake. *Episodes*, 31(3):291–301, 2008.

[77] Y Yanagisawa, I Kobayashi, K Takeuchi, M Tateishi, K Chihara, and H Kato. Geology of the Ojiya district, with geological sheet map at 1:50:000. *Geological Survey of Japan*, 1986.

[78] Q Zaruba and Mencl V. 1969: Landslides and their control. 1969.

[79] Weihua Zhang and David R Montgomery. Digital elevation model grid size, landscape representation, and hydrologic simulations. *Water Resources Research*, 30(4):1019–1028, 1994.